J. Fluid Mech. (2013), *vol.* 737, *pp.* 280–307.
doi:10.1017/jfm.2013.554

On the active feedback control of a swirling flow in a finite-length pipe

Shixiao Wang[1,†], Zvi Rusak[2], Steve Taylor[1] and Rui Gong[1]

[1]Department of Mathematics, University of Auckland, 38 Princes Street, Auckland, 1142, New Zealand

[2]Department of Mechanical, Aerospace and Nuclear Engineering, Rensselaer Polytechnic Institute, Troy, NY 12180-3590, USA

(Received 28 December 2012; revised 6 October 2013; accepted 15 October 2013; first published online 25 November 2013)

The physical properties of a recently proposed feedback-stabilization method of a vortex flow in a finite-length straight pipe are studied for the case of a solid-body rotation flow. In the natural case, when the swirl ratio is beyond a certain critical level, linearly unstable modes appear in sequence as the swirl level is increased. Based on an asymptotic long-wave (long-pipe) approach, the global feedback control method is shown to enforce the decay in time of the perturbation's kinetic energy and thereby quench all of the instability modes for a swirl range above the critical swirl level. The effectiveness of an extended version of this feedback flow control approach is further analysed through a detailed mode analysis of the full linear control problem for a solid-body rotation flow in a finite-length pipe that is not necessarily long. We first rigourously prove the asymptotic decay in time of all modes with real growth rates. We then compute the growth rate and shape of all modes according to the full linearized control problem for swirl levels up to 50 % above the critical level. We demonstrate that the flow is stabilized in the whole swirl range and can be even further stabilized for higher swirl levels. However, the control effectiveness is sensitive to the choice of the feedback control gain. A potentially best range of the gain is identified. An inadequate level of gain, either insufficient or excessive, could lead to a marginal control or failure of the control method at high swirl levels. The robustness of the proposed control law to stabilize both initial waves and continuous inlet flow perturbations and the elimination of the vortex breakdown process are demonstrated through numerical computations.

Key words: control theory, vortex breakdown, vortex instability

1. Introduction

The discovery of the vortex breakdown phenomenon in the leading-edge vortices above slender wings at high angles of incidence (Peckham & Atkinson 1957) stimulated extensive research on the dynamics of swirling flows in open or confined configurations for over half a century (Benjamin 1962; Sarpkaya 1971; Hall 1972; Leibovich 1978, 1984; Delery 1994; Brücker & Althaus 1995; Sarpkaya 1995; Wang & Rusak 1997; Mattner, Joubert & Chong 2002). This phenomenon is characterized by

† Email address for correspondence: wang@math.auckland.ac.nz

a sudden and abrupt change of the flow structure when the upstream vortex flow swirl ratio ω (the ratio of the maximum circumferential velocity over the characteristic axial velocity) exceeds a critical value. The flow decelerates along the vortex axis and a free stagnation point is formed, followed by a large separation zone and turbulence behind it. The breakdown states range from spiral waves and axisymmetric bubbles that may coexist at low-Reynolds-number flows ($Re < 10^4$) to axisymmetric, near-stagnant, semi-infinite zones at high-Re swirling flows ($Re > 5 \times 10^4$).

The vortex breakdown phenomenon has either detrimental or beneficial effects on a variety of real flow applications such as the aerodynamics of modern fighter aircraft and missiles or flame stabilization in gas-turbine combustors. The control of vortex breakdown is a practically important problem for these technologies, either to prevent breakdown or to promote it. For example, the delay of breakdown in leading-edge vortices can improve aircraft aerodynamic performance and widen their operational envelope of flight (Delery 1994) while a stable induction of breakdown can enhance lean-premixed combustion with low emissions (Paschereit & Gutmark 2002; Muruganandam *et al.* 2005; Knole & Sattelmayer 2009). Mitchell & Delery (2001) reviewed the various available control approaches of vortex breakdown in leading-edge vortices. They concluded that none of the techniques has clearly demonstrated a superior efficiency or effectiveness in controlling either the breakdown structure or its location. They emphasized that for an effective control strategy of the vortex breakdown phenomenon it is important to understand the stages of flow evolution leading to a vortex breakdown state including the internal flow mechanisms that destabilize a concentrated vortex. Similarly, Muruganandam *et al.* (2005) developed an active flow control technique of a swirl-stabilized lean-premixed combustion in a chamber and emphasized that the combustor's nominal dynamics and flow oscillations without control have an important impact on the effectiveness of the active control system.

In this paper we develop a control theory of the vortex breakdown process in a pipe flow. It is based on the physical mechanism leading to breakdown in high-Re swirling flows in a finite-length, straight circular pipe that was established by Wang & Rusak (1997) and Rusak *et al.* (2012). In this fundamental study, the base flow is assumed to be an inviscid columnar axisymmetric swirling flow in a circular pipe with realistic physical, non-periodic conditions specified at the pipe inlet and outlet. Fixed-in-time profiles of the axial velocity, circumferential velocity and azimuthal vorticity are set at the inlet and a state with no axial changes is set at the outlet. These conditions represent a physical set-up of swirling flows in a pipe generated by a fixed-in-place and fixed-in-time vortex generator ahead of the pipe in a steady, continuous and smooth operation as found in the experimental set-ups of Sarpkaya (1971), Faler & Leibovich (1977), Leibovich (1978, 1984), Garg & Leibovich (1979) and Mattner *et al.* (2002). A similar set of boundary conditions is used in all numerical simulations of the vortex breakdown (see, for example, Beran 1994, Lopez 1994, Snyder & Spall 2000 and Meliga & Gallaire 2011). In particular, Snyder & Spall (2000) demonstrated that simulation of the flow in a pipe including the vortex generator region ahead of it (which is based on the experimental set-up of Sarpkaya 1995) and simulation of the flow in the pipe alone (with fixed-in-time inlet axial and circumferential velocity profiles taken from the full apparatus simulation) give same results and show agreement with the experimental measurements. This result supports our approach of setting the inlet and outlet conditions.

Within this physical model, the theory of vortex breakdown was derived by Wang & Rusak (1996, 1997). Two critical swirl ratios, denoted by ω_0 and ω_1 were

identified, where $\omega_0 < \omega_1$. These critical swirl ratios connect between three branches of equilibrium states. Columnar vortex flow states with $0 < \omega < \omega_1$ are asymptotically stable while states with $\omega > \omega_1$ are unstable. This instability mechanism cannot be predicted by the classical vortex flow stability studies of Kelvin (1880) and Rayleigh (1916). Solitary-wave states along the branch connecting between ω_0 and ω_1 are also unstable. Stable breakdown states appear when $\omega > \omega_0$. The vortex breakdown process was shown to be a direct consequence of the loss of stability of the base columnar flow related with the upstream propagation of azimuthal vorticity and circulation waves and their interaction with the fixed inlet (upstream) state. This is followed by a necessary and fast transition to a stable breakdown state with a long and large separation (near-stagnation) zone around the vortex centreline when $\omega > \omega_0$. The effects of slight viscosity, weak inlet vorticity perturbations and small variations in the pipe geometry were treated as perturbations from the base case and extended the theory to realistic apparatuses.

The Wang & Rusak theory of vortex stability and breakdown was verified by the numerical simulations of Rusak, Whiting & Wang (1998) and Rusak *et al.* (2012). It also showed nice agreement with the direct numerical simulations of Beran & Culick (1992), Beran (1994) and Lopez (1994). The recent bifurcation and stability studies of Meliga & Gallaire (2011) support the theory as well. The theoretical predictions are also consistent with the experimental results of the breakdown of vortices in pipes by Leibovich (1984), Sarpkaya (1995) and Mattner *et al.* (2002) (see Rusak *et al.* 1998) and in leading-edge vortices above slender delta wings by O'Neil *et al.* (1989) (see Rusak & Lamb 1999).

Moreover, the recent study by Rusak *et al.* (2012) reveals the complicated dynamical behaviour of the evolution of perturbations in a swirling flow when ω is around ω_1. Using a long-wave (long-pipe) approach, a nonlinear model equation has been derived and subjected to the non-periodic inlet/outlet conditions. This approach extends the model problem of Leibovich & Randall (1972). The computed dynamics using this model problem shows a quantitative agreement with results from numerical simulations that are based on the axisymmetric Euler equations for various swirl levels around ω_1 and as long as perturbations are small. Examples of the flow evolution in response to different initial perturbations demonstrate the various stages of the flow dynamics, specifically during the transition to vortex breakdown states. They revealed the initial linear growth stage of perturbations with fixed growth rate and linear mode shape followed by a weakly nonlinear growth stage of evolution of faster-than-exponential and shape-changing modes, a nonlinear transition stage to a breakdown state, and a stage of decay to a breakdown state. The explosive modes during the weakly nonlinear growth stage provide the sudden and abrupt nature of the vortex breakdown phenomenon which may be difficult to robustly control using any method that does not account for these waves. Wang & Rusak (2011) showed that the feed-forward interaction between the inlet radial velocity and the perturbation growth in the bulk is the major physical mechanism for the production of the perturbation's kinetic energy and the formation of instability and the explosive nonlinear modes. Also, Rusak *et al.* (2012) found that in near solid-body rotation flows with large vortical cores, the perturbation dynamics is mostly in the linear stage of growth. However, in concentrated vortices with small cores, relevant small initial perturbations exhibit a fast weakly nonlinear growth stage from the beginning. The purpose of this study is to identify a control method that can cut this feed forward mechanism by actively inducing feedback control commands that reduce the inlet radial velocity and may stabilize the flow and eliminate the breakdown process.

The Wang & Rusak instability of columnar vortex flows when $\omega > \omega_1$ followed by the weakly nonlinear explosive modes are crucial elements in deriving a control methodology of vortex flows in pipes. Gallaire, Chomaz & Huerre (2004) extended the Wang & Rusak instability to higher swirl levels and showed for a solid-body rotation flow the important fact that unstable modes appear in sequence as swirl ratio ω is increased above ω_1. Wang (2008) and Rusak *et al.* (2012) extended this result to vortices with finite-size cores. It is therefore clear that to prevent the columnar base flow from evolving to a breakdown state, it is necessary to quench all of the unstable modes of perturbations that arise in a swirling flow when $\omega > \omega_1$.

Using tools from optimal linear control theory with a certain cost function that involves the perturbation's size and the control power, Gallaire *et al.* (2004) developed a feedback control scheme to suppress the linear development of the Wang & Rusak instability. However, their approach is based on describing the flow perturbations from the columnar state by a finite set of stability modes. As a result, their flow stabilization scheme is limited to a small range ($\sim$7%) of the swirl ratio above ω_1, i.e. the higher the swirl ratio is, the more difficult it is to suppress the instability modes that appear in sequence, and at a certain swirl ratio, control is lost.

Recently, Meliga & Gallaire (2011) studied a passive control technique of the axisymmetric vortex breakdown in a constricted pipe using low flow-rate jets positioned at the pipe wall to modify the base swirling flow. Nonlinear branches of steady near-columnar states, solitary wave states, and breakdown states connected by two critical fold points were computed using the Navier–Stokes equations. The linear stability modes of these states were also calculated and agree with Wang & Rusak vortex breakdown theory. Depending on the jets position, the first appearance of breakdown was either delayed by $\sim$12% with respect to the natural case or the range of hysteresis loop was alleviated. However, this approach does not include any dynamically active feedback stabilization of the flow.

The long-wave model of Rusak *et al.* (2012), which captures the essential perturbation dynamics in a rather simple form, is a powerful tool for the study of vortex flow control. Using this model, they have proposed and rigourously proved a robust feedback stabilization strategy to enforce the decay of perturbations on a swirling flow in a pipe in the linear growth stage. This method feeds back inlet radial velocity information to the controller (for example, dynamical variation of pipe radius or wall jet injection) and globally suppresses *all* the unstable modes of the flow when $\omega > \omega_1$. They also found that with sufficient control gain this active control strategy is able to overcome the destabilizing nonlinear steepening effects and enforce the decay of perturbations in the fast weakly-nonlinear stage of flow dynamics as well. The use of this method for large and medium core-size vortices shows that it is applicable to stabilizing the flows at above critical swirl levels for a wide range of swirl and with realistic initial disturbances. For small core-size concentrated vortex flows, this feedback control approach becomes more sensitive to realistic initial disturbances and there is a need to increase the control gain to stabilize the flow.

In this paper, we develop a theoretical foundation of the active control methodology proposed by Rusak *et al.* (2012). We focus on analytically describing the control properties in the linear growth stage of perturbations by studying the case of a base flow given by a solid body rotation flow. This flow case provides analytical simplicity that is used to reveal the details of the control mechanism. The results are directly applicable through rescaling of parameters to the control of vortices with large, medium and small core sizes in their linear growth stage of perturbations. The results

may also be relevant toward the control of perturbations in the weakly nonlinear growth stage or even large perturbations (see Xu 2012).

The outline of the paper is as follows. In § 2 we present the mathematical problem formulation for the dynamics of an inviscid, axisymmetric, swirling flow in a finite-length pipe. In § 3.1 we derive the linear dynamics problem for a perturbation on a solid-body rotation flow in the pipe. We also reduce the problem to the case of a long-wave dynamics in a long pipe. In § 3.2 we show the correlation between the long-wave linear stability modes to those of the full linear dynamics of the solid-body flow in a finite-length pipe. In § 4.1 we first use the long-pipe model to generalize the feedback control strategy of Rusak *et al.* (2012) and include a wider range of outlet conditions relevant to various physical settings. In § 4.2 we study the effect of the control gain on the stability growth rates of the eigenmodes of the controlled long-wave linear problem. We show that the use of too small gain or too large gain may cause marginal control. In § 4.3, we extend the feedback control approach to the full linear dynamics problem in a finite-length pipe and establish a fundamental energy identity. In § 4.4 we compute the linear growth rates according to the full linear control problem and show that insufficient or excessive feedback control gain leads to uncontrolled situations when swirl is increased, while a certain range of gain provides a robust control for a wide range of swirl above critical. In § 4.5 we discuss the relationship between the eigenmodes shape and the gain and shed light on the physical mechanism of the proposed feedback stabilization methodology of swirling flows. In § 4.6 we study the robustness of the control approach to inlet perturbations. The paper conclusions are summarized in § 5.

2. Problem formulation

2.1. *Mathematical model*

We consider an incompressible, inviscid and axisymmetric flow in a straight, finite-length, circular pipe. Cylindrical coordinates (r, θ, x) are used where (u, v, w) are the radial, azimuthal and axial velocity components, respectively. Axial and radial distances x and r are scaled with the pipe radius and pipe non-dimensional length is L, $0 \leqslant x \leqslant L$ and $0 \leqslant r \leqslant 1$. Velocity components are scaled with the characteristic axial speed entering the pipe. Time t is scaled with the ratio of pipe radius to inlet characteristic speed. Let $y = r^2/2$ where $0 \leqslant y \leqslant 1/2$. By virtue of the axisymmetry, a stream function $\psi(x, y, t)$ can be defined such that $u = -\psi_x/\sqrt{2y}$ and $w = \psi_y$. The reduced form of azimuthal vorticity is $\chi = -(\psi_{yy} + \psi_{xx}/2y)$ (where the azimuthal vorticity is $\eta = \sqrt{2y}\chi$). The circulation function $K(x, y, t)$ is defined as $K = rv = \sqrt{2y}v$. The equations which relate the evolution of $\psi(x, y, t)$, $\chi(x, y, t)$ and $K(x, y, t)$ are the unsteady Squire–Long equations (Squire 1960; Long 1953):

$$K_t + \psi_y K_x - \psi_x K_y = 0, \tag{2.1a}$$

$$\chi_t + \psi_y \chi_x - \psi_x \chi_y = \frac{K K_x}{2y^2}. \tag{2.1b}$$

The first equation (2.1*a*) is the transport equation of flow circulation along a path line. The second equation (2.1*b*) describes the interaction between the convection of the reduced azimuthal vorticity χ along a path line and vorticity stretching by the axial gradient of the circulation. The later effect is swirl dependent and generates swirl-driven waves that can propagate either downstream or upstream and interact with the pipe inlet and outlet conditions. This interaction may lead to flow instability.

We consider the dynamics of a flow governed by (2.1) under certain realistic boundary conditions that represent a physical setting of a swirling flow in a finite-length pipe that is generated by a vortex generator ahead of the pipe (Wang & Rusak 1997; Rusak *et al.* 2012). We set for all $t \geqslant 0$:

$$\psi(x, 0, t) = 0, \quad \psi(x, \tfrac{1}{2}, t) = \psi_0(\tfrac{1}{2}) \quad \text{for } 0 \leqslant x \leqslant L, \tag{2.2a}$$

$$\psi(0, y, t) = \psi_0(y), \quad \psi_{xx}(0, y, t) = 0, \quad K(0, y, t) = \omega K_0(y) \quad \text{for } 0 \leqslant y \leqslant \tfrac{1}{2}, \tag{2.2b}$$

$$\psi_x(L, y, t) = 0 \quad \text{for } 0 \leqslant y \leqslant \tfrac{1}{2}. \tag{2.2c}$$

In this setting, the profiles of the axial and circumferential velocity components are assumed to be fixed for all time t at the pipe inlet and are specified by the flow flux stream function $\psi_0(y)$ and the circulation function $\omega K_0(y)$, respectively, where ω is the incoming flow swirl ratio. Note that the reduced azimuthal vorticity at the inlet $\chi(0, y, t)$ is also fixed for all time since we set $\psi_{xx}(0, y, t) = 0$. Also, the flow has a degree of freedom to develop at any instant an inlet radial velocity in response to perturbations in the bulk that tend to cast such an influence. The outlet boundary condition is set by a zero radial velocity for all time. This rather passive condition is relevant for a sufficiently long pipe (where $L \gg 1$). A similar set of boundary conditions is used in all of the numerical simulations of the vortex breakdown phenomenon (see, among others, Beran 1994, Lopez 1994, Snyder & Spall 2000 and Meliga & Gallaire 2011). In the discussion in § 4 we will also consider a fixed flux outlet condition and more general outlet conditions that may represent realistic settings in short pipes. The problem defined by (2.1) and assumed boundary conditions (2.2) is well posed and, using relevant initial conditions for the stream function, circulation and azimuthal vorticity, describes the axisymmetric evolution of a swirling flow in a finite-length pipe.

The columnar flow

$$\psi(x, y, t) = \psi_0(y), \quad K(x, y, t) = \omega K_0(y), \quad \chi(x, y, t) = -\psi_{0yy}(y), \tag{2.3}$$

is a base steady-state solution of the problem for all time $t \geqslant 0$ and every level of ω. We look to describe the dynamics of disturbances on this base flow and its control.

In present paper, we focus on a base flow which is combined of solid-body rotation and uniform axial flow. For this base flow $\psi_0(y) = y$ and $K_0(y) = 2y$. The solid-body rotation flow provides analytical simplicity through which the linear stability modes of the natural flow as well as of the controlled flow can be studied and characterized in an explicit way. In the more global scope, the solid-body rotation flow represents the essence of the linearized dynamics of general base flow vortices with finite size vortical cores in a finite-length pipe, see Wang & Rusak (1996) and Rusak *et al.* (2012). In the special case of the long-wave linearized dynamics of perturbations, the solution for the solid body rotation flow can be rescaled to provide the long-wave dynamics of a general base swirling flow in the pipe. Moreover, the solid body rotation flow can be considered as a nominal base flow for which the dynamics of perturbation stays linear even when the perturbation size is relatively large, see Rusak *et al.* (2012).

In the classical linear stability analysis, the perturbation is described by a linear combination of sinusoidal Fourier modes. This approach is limited in scope to a flow in an ideal, infinitely long pipe or to a finite-length pipe with periodic inlet–outlet conditions, where translation invariance is natural. In fact, axisymmetric perturbation on the solid-body rotation flow lacks any growth mechanism including transient growth, see Wang (2009). This shows the limitations of the classical stability theory and its scope of application. On the other hand, when the flow evolves in

a finite-length pipe from a vortex generator ahead of the pipe into the pipe outlet, the translation invariance does not exist. All experimental apparatuses that study vortex stability and breakdown show a difference between the inlet and outlet states. Therefore, this gives rise to a different set of stability modes that account for the different set of the boundary conditions of the flow in finite length pipe.

3. Linear stability of the solid-body rotation flow

3.1. *Linearized dynamics of the solid-body rotation flow*

In the derivation of the governing equation for the linearized dynamics of the solid-body rotation flow, we introduce

$$\psi(x, y, t) = y + \epsilon\psi_1(x, y, t) + \cdots, \tag{3.1a}$$

$$K(x, y, t) = 2\omega y + \epsilon K_1(x, y, t) + \cdots, \tag{3.1b}$$

where $0 < |\epsilon| \ll 1$, and ψ_1 and K_1 are the stream function and circulation disturbances, respectively. Substituting (3.1) into the governing equations (2.1) and ignoring second-order $O(\epsilon^2)$ terms we arrive at the linearized equations of motion:

$$K_{1t} + K_{1x} - 2\omega\psi_{1x} = 0, \tag{3.2a}$$

$$-\frac{\omega}{y}K_{1x} + \chi_{1t} + \chi_{1x} = 0, \tag{3.2b}$$

where χ_1 is the reduced azimuthal vorticity disturbance: $\chi_1 = -(\psi_{1yy} + \psi_{1xx}/2y)$. The perturbations $\psi_1(x, y, t)$ and $K_1(x, y, t)$ must satisfy a set of boundary conditions derived from (2.2):

$$\psi_1(x, 0, t) = 0, \quad \psi_1(x, \tfrac{1}{2}, t) = 0 \quad \text{for } 0 \leqslant x \leqslant L, \tag{3.3a}$$

$$\psi_1(0, y, t) = 0, \quad \psi_{1xx}(0, y, t) = 0, \quad K_1(0, y, t) = 0 \quad \text{for } 0 \leqslant y \leqslant \tfrac{1}{2}, \tag{3.3b}$$

$$\psi_{1x}(L, y, t) = 0 \quad \text{or } \psi_1(L, y, t) = 0 \quad \text{for } 0 \leqslant y \leqslant \tfrac{1}{2}. \tag{3.3c}$$

From (3.2) we find that

$$K_{1t} = -\frac{y}{\omega}(\chi_{1t} + \chi_{1x}) + 2\omega\psi_{1x} \tag{3.4}$$

and, thus, the inlet condition $K_1(0, y, t) = 0$ is replaced by

$$y\psi_{1yyx}(0, t) + \tfrac{1}{2}\psi_{1xxx}(0, t) + 2\omega^2\psi_{1x}(0, t) = 0. \tag{3.5}$$

A manipulation of (3.2) (see Wang & Rusak 1996) leads to a linear partial differential equation which governs the evolution of the stream function perturbation $\psi_1(x, y, t)$:

$$\left(\psi_{1yy} + \frac{\psi_{1xx}}{2y}\right)_{xx} + 2\left(\psi_{1yy} + \frac{\psi_{1xx}}{2y}\right)_{xt} + \left(\psi_{1yy} + \frac{\psi_{1xx}}{2y}\right)_{tt} + \frac{2\omega^2}{y}\psi_{1xx} = 0. \tag{3.6}$$

The solution of (3.6) must satisfy boundary conditions (3.3) and (3.5).

Let $\Omega = 4\omega^2$. It is a remarkable fact that (3.6) allows a solution with axial and radial variables separated, in the form of the linear combination of the modes $\psi_{1n}(x, y, t) = \phi_{Bn}(y)\varphi_n(x, t)$ (n is a positive integer). Here the function $\phi_{Bn}(y)$ are the radial modes determined by Benjamin's (1962) eigenvalue problem:

$$\phi_{Bnyy} + \frac{\Omega_{Bn}}{2y}\phi_{Bn} = 0, \tag{3.7a}$$

$$\phi_{Bn}(0) = \phi_{Bn}(1/2) = 0. \tag{3.7b}$$

The solution of (3.7) gives the eigenvalues $\Omega_{Bn} = 4\omega_{Bn}^2 = (j_{1,n})^2$, where $j_{1,n}$ is the nth zero of the Bessel function $\mathrm{J}_1(Z)$ and the eigenfunction $\phi_{Bn}(y) = \sqrt{2y}\mathrm{J}_1(\sqrt{2\Omega_{Bn}y})$.

In the present paper we focus on the range of swirl $0 \leqslant \omega \leqslant 3$ which includes Benjamin's specific swirl $\omega_B = \omega_{B1} = 1.915855$ but does not include Benjamin's second critical swirl $\omega_{B2} = 3.507795$ and higher. In this range of swirl only the first mode in the series $\psi_1(x, y, t) = \phi_B(y)\varphi(x, t)$ is of interest in terms of change of stability properties, where $\phi_B(y) = \phi_{B1}(y)$ and $\varphi(x, t) = \varphi_1(x, t)$. In this swirl range, all other higher-order modes are asymptotically stable with very negative growth rates and the perturbations related to these modes quickly decay. Substituting $\psi_1(x, y, t)$ into (3.6), we obtain the equation that describes the linear dynamics of the perturbation:

$$\varphi_{xxxx} + (\Omega - \Omega_B)\varphi_{xx} + 2\varphi_{xxxt} + \varphi_{xxtt} - 2\Omega_B\varphi_{xt} - \Omega_B\varphi_{tt} = 0. \tag{3.8}$$

The boundary conditions (3.3) and (3.5) become

$$\varphi(0, t) = \varphi_{xx}(0, t) = 0, \quad \varphi_{xxx}(0, t) + (4\omega^2 - \Omega_B)\varphi_x(0, t) = 0, \quad \varphi_x(L, t) = 0. \tag{3.9}$$

Let $\epsilon_1 = 1/L^2$, $X = \sqrt{\epsilon_1}x$ and $t^* = \epsilon_1^{3/2}t$. We write $\varphi(x, t)$ in terms of the rescaled variables, $\varphi(x, t) = \mathscr{A}(X, t^*)$. Then, the linear dynamics equation (3.8) can be written as

$$-2\Omega_B\mathscr{A}_{Xt^*} + \mathscr{A}_{XXXX} + 4\kappa_\omega\mathscr{A}_{XX} + 2\epsilon_1\mathscr{A}_{XXXt^*} + \frac{4\kappa_\omega^2\epsilon_1}{\Omega_B}\mathscr{A}_{XX} + \epsilon_1^2\mathscr{A}_{XXt^*t^*} - \epsilon_1\Omega_B\mathscr{A}_{t^*t^*} = 0. \tag{3.10}$$

Here, $\kappa_\omega = 2\omega_B(\omega - \omega_B)/\epsilon_1$. The boundary conditions for all $t^* \geqslant 0$ are

$$\mathscr{A}(0, t^*) = 0, \quad \mathscr{A}_{XX}(0, t^*) = 0, \quad \mathscr{A}_{XXX}(0, t^*) + \left(4\kappa_\omega + \frac{4\kappa_\omega^2\epsilon_1}{\Omega_B}\right)\mathscr{A}_X(0, t^*) = 0$$
$$\text{and} \quad \mathscr{A}_X(1, t^*) = 0. \tag{3.11}$$

In the case of a long pipe where $L^2 \gg 1$ we have $\epsilon_1 \sim 0$. Then, when terms of order ϵ_1 and higher are neglected, equation (3.10) can be simplified to

$$2\Omega_B\mathscr{A}_{Xt^*} = \mathscr{A}_{XXXX} + 4\kappa_\omega\mathscr{A}_{XX}, \tag{3.12}$$

and the boundary conditions (3.11) reduce to

$$\mathscr{A}(0, t^*) = 0, \quad \mathscr{A}_{XX}(0, t^*) = 0, \quad \mathscr{A}_{XXX}(0, t^*) + 4\kappa_\omega\mathscr{A}_X(0, t^*) = 0$$
$$\text{and} \quad \mathscr{A}_X(1, t^*) = 0. \tag{3.13}$$

Integrating (3.12) with respect to X and using the boundary conditions (3.13) gives the long-wave perturbation problem:

$$2\Omega_B\mathscr{A}_{t^*} = \mathscr{A}_{XXX} + 4\kappa_\omega\mathscr{A}_X, \tag{3.14}$$

with the boundary conditions

$$\mathscr{A}(0, t^*) = 0, \quad \mathscr{A}_{XX}(0, t^*) = 0 \quad \text{and} \quad \mathscr{A}_X(1, t^*) = 0. \tag{3.15}$$

3.2. *Growth rates of linear stability modes according to problem (3.10) and (3.11) and to the long-wave problem (3.14) and (3.15)*

To study the linear stability of the solid-body rotation flow based on the problem (3.10) and (3.11), we assume a mode $\mathscr{A}(X, t^*) = \tilde{\mathscr{A}}(X)\mathrm{e}^{\sigma^* t^*}$, where $\tilde{\mathscr{A}}(X)$ is the perturbation's mode shape function and $\sigma^* = \sigma/\epsilon_1^{3/2}$ is the perturbation's rescaled growth rate. Inserting it into (3.10) and (3.11) one obtains the linear eigenvalue

problem

$$\tilde{\mathscr{A}}_{XXXX} + 4\kappa_\omega \tilde{\mathscr{A}}_{XX} - 2\Omega_B \sigma^* \tilde{\mathscr{A}}_X + 2\epsilon_1 \sigma^* \tilde{\mathscr{A}}_{XXX} + \frac{4\kappa_\omega^2 \epsilon_1}{\Omega_B} \tilde{\mathscr{A}}_{XX} + \epsilon_1^2 \sigma^{*2} \tilde{\mathscr{A}}_{XX} - \epsilon_1 \Omega_B \sigma^{*2} \tilde{\mathscr{A}} = 0. \tag{3.16a}$$

$$\tilde{\mathscr{A}}(0) = 0, \quad \tilde{\mathscr{A}}_{XX}(0) = 0, \quad \tilde{\mathscr{A}}_{XXX}(0) + \left(4\kappa_\omega + \frac{4\kappa_\omega^2 \epsilon_1}{\Omega_B}\right) \tilde{\mathscr{A}}_X(0) = 0 \quad \text{and} \quad \tilde{\mathscr{A}}_X(1) = 0. \tag{3.16b}$$

Similarly, the long-wave linear stability problem of the solid-body rotation flow based on (3.14) and (3.15) becomes

$$\tilde{A}_{XXX} + 4\kappa_\omega \tilde{A}_X - 2\Omega_B \sigma^* \tilde{A} = 0, \tag{3.17a}$$

$$\tilde{A}(0) = 0, \quad \tilde{A}_{XX}(0) = 0 \quad \text{and} \quad \tilde{A}_X(1) = 0. \tag{3.17b}$$

Note that the eigenvalue problem (3.16) is a fourth-order differential equation with four boundary conditions. On the other hand, the eigenvalue problem (3.17) is a cubic order differential equation with three boundary conditions. Only when ϵ_1 is sufficiently small, we can neglect the high-order terms, integrate it with respect to X and use the third inlet condition in (3.16*b*) to obtain (3.17*a*).

The two eigenvalue problems (3.16) and (3.17) are solved by a shooting method using a standard fourth-order accurate Runge–Kutta solver. The growth rates σ are then calculated from the scaling relationship $\sigma = \epsilon_1^{3/2} \sigma^*$. The results of Gallaire *et al.* (2004) for a pipe length $L = 10$ match with our present computation for this pipe length.

Solutions in figure 1 for the case of a pipe with a non-dimensional length $L = 6$ ($\epsilon_1 = 1/36$) show the appearance of linearly unstable modes in sequence as swirl is increased above the first critical level for a finite-length pipe $\omega_1 = \sqrt{\omega_B^2 + \pi^2/(16L^2)}$ (first defined in Wang & Rusak 1996). The results from the full linear stability problem are the same as those found analytically by Wang & Rusak (1996) in their stability analysis. In these computations $L = 6$ is a typical pipe length of the experimental apparatuses (Garg & Leibovich 1979). The results reflect the general stability behaviour for a similar length of the pipe.

Figure 1(*a*) shows a comparison of the growth rates of the least stable mode computed from the linear stability problem (3.16) and from the long-wave linear stability problem (3.17) for the range $1.91 < \omega < 1.96$. It can be seen that in this range of swirl only one mode becomes unstable when $\omega > \omega_1 = 1.920$. The growth rates from both computations are real values and exhibit a very small numerical difference. Figure 1(*b*) shows a comparison of the computed results of the real part of σ for the two unstable modes that appear in the range $1.96 < \omega < 2.02$ with complex conjugate values, and the three unstable modes that appear in the range $2.02 < \omega < 2.15$. The difference between results increases as the swirl level increases but the growth rate lines stay similar in the swirl range. This demonstrates the applicability of the long-wave problem (3.14) and (3.15) to the full perturbation's linear dynamics in a range of swirl above the critical swirl ω_1.

4. The feedback stabilization of the solid-body rotation flow

4.1. *The feedback control using the long-wave linear dynamics*

A feedback control strategy is proposed by Rusak *et al.* (2012) to quench the unstable evolution of a perturbed columnar swirling flow in a long but finite-length pipe with

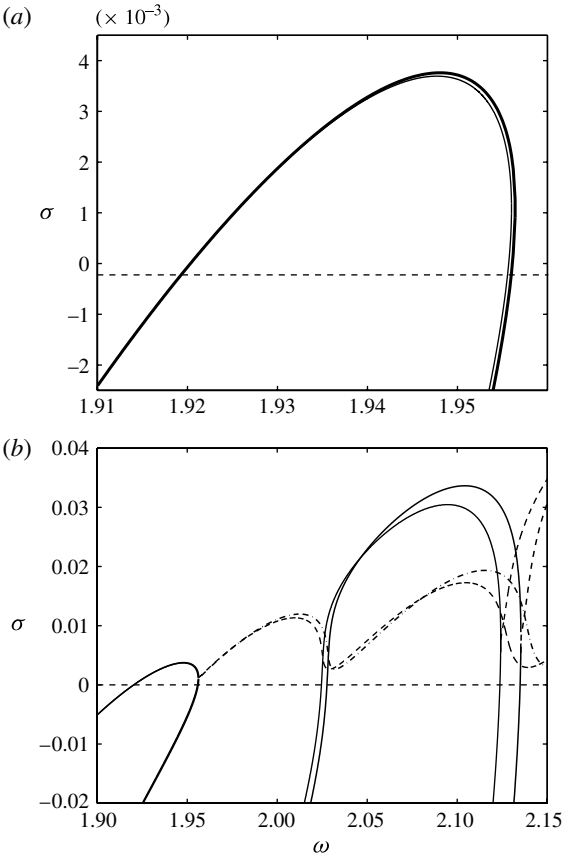

FIGURE 1. Growth rate σ comparison: (*a*) the swirl ratio range with one unstable mode; (*b*) the swirl ratio range with three unstable modes. The thick lines are results of the full linear stability problem (3.16) and the thin lines, the results of the long-wave linear stability problem (3.17). The solid lines are real growth rates and the dashed lines are the real part of complex growth rates.

non-periodic boundary conditions. A generalization of this control law is presented as follows. We consider a control term $c(X)u(t^*)$, where $c(X)$ is a fixed function representing the control profile along the axial direction, added to the governing equation (3.14) with modified and more general outlet conditions, i.e.

$$2\Omega_B A_{t^*} = A_{XXX} + 4\kappa_\omega A_X + c(X)u(t^*) \quad \text{for } 0 \leqslant X \leqslant 1,\ t^* > 0, \tag{4.1a}$$

$$A(0, t^*) = A_{XX}(0, t^*) = 0, \quad c_1 A_X(1, t^*) + c_2 A(1, t^*) = 0 \quad \text{for } t^* > 0, \tag{4.1b}$$

$$A(X, 0) = f(X) \quad \text{for } 0 \leqslant X \leqslant 1. \tag{4.1c}$$

Here $c_1 \geqslant 0$, $c_2 \geqslant 0$ and $c_1 + c_2 = 1$.

The control term represents control commands using swirl changes at the inlet (see § 4.3), pipe geometry changes from a straight pipe (see Xu 2012), or wall injection commands. We will show that $u(t^*)$, with a control profile function $c(X) = 1 - c_2 X$, can be determined by the inlet flow state $A_X(0, t^*)$ for all time t^* so that the perturbation decays in time and flow is stabilized. In appendix A we prove a fundamental theorem for the feedback stabilization of a swirling flow in a finite-length pipe when $\kappa_\omega > 0$.

Let

$$\tilde{E}(t^*) = \frac{1}{2}\int_0^1 (A_X)^2 \, \mathrm{d}X \tag{4.2}$$

be the perturbation's kinetic energy (associated with the radial velocity) and

$$\hat{E}(t^*) = \frac{1}{2}\int_0^1 (A_X)^2 \, \mathrm{d}X + \frac{c_2}{c_1} A_X(1, t^*)^2 \tag{4.3}$$

be the extended perturbation's kinetic energy with $c_1 \neq 0$. Then, when either $c_1 = 1$ and $c_2 = 0$ or $c_1 = 0$ and $c_2 = 1$, the following energy identity holds

$$2\Omega_B \frac{\mathrm{d}\tilde{E}}{\mathrm{d}t^*} = -\frac{1}{2}(A_{XX}(1, t^*))^2 - 2\kappa_\omega (A_X(1, t^*))^2 + 2\kappa_\omega (A_X(0, t^*))^2 + A_X(0, t^*)u(t^*). \tag{4.4}$$

Also, when $c_1 > 0$, $c_2 > 0$ and $c_1 + c_2 = 1$, the following extended energy identity holds,

$$2\Omega_B \frac{\mathrm{d}\hat{E}}{\mathrm{d}t^*} = -\frac{1}{2}(A_{XX}(1, t^*))^2 - 2\kappa_\omega (A_X(1, t^*))^2 + 2\kappa_\omega (A_X(0, t^*))^2 + A_X(0, t^*)u(t^*). \tag{4.5}$$

Note that the right-hand sides of (4.4) and (4.5) are the same. The first term on the right-hand side of (4.4) (or (4.5)), which originates from the dispersion term in (4.1), is always stabilizing the flow. The second and third terms on the right-hand side of (4.4) (or (4.5)) depend on the swirl ratio with respect to Benjamin's critical level. The second term has a stabilizing effect when $\omega > \omega_B$ ($\kappa_\omega > 0$). The third term is destabilizing when $\omega > \omega_B$ ($\kappa_\omega > 0$). Wang & Rusak (2011) showed that in the natural case without control, $A_X(0, t^*)^2 > A_X(1, t^*)^2$ for the unstable modes when $\omega > \omega_1$. The overall combined effect of the second and third terms is destabilizing. There is a feed-forward mechanism between the inlet and the perturbation's kinetic energy in the flow bulk which destabilizes the flow. For a stabilizing effect of the control action when $\kappa_\omega > 0$, the control function $u(t^*)$ must be sufficiently large for all time to overcome the destabilizing effect from the third term. Assuming the active feedback-control law

$$u(t^*) = -2\gamma\kappa_\omega A_X(0, t^*), \tag{4.6}$$

Equations (4.4) and (4.5) become, respectively,

$$\Omega_B \frac{\mathrm{d}\tilde{E}}{\mathrm{d}t^*} \leqslant \kappa_\omega (1 - \gamma)(A_X(0, t^*))^2, \tag{4.7}$$

and

$$\Omega_B \frac{\mathrm{d}\hat{E}}{\mathrm{d}t^*} \leqslant \kappa_\omega (1 - \gamma)(A_X(0, t^*))^2. \tag{4.8}$$

Thus, $\mathrm{d}\tilde{E}/\mathrm{d}t^*$ or $\mathrm{d}\hat{E}/\mathrm{d}t^*$ are negative for all $t^* > 0$ when $\gamma > 1$. The active feedback control cuts the natural feed-forward instability mechanism to stabilize the flow when $\omega > \omega_1$. This leads to the following control results for various settings of the outlet boundary conditions.

Case 1. For boundary conditions given by

$$A(0, t^*) = A_{XX}(0, t^*) = 0 \quad \text{and} \quad A_X(1, t^*) = 0 \quad \text{for } t^* > 0, \tag{4.9}$$

the energy $\tilde{E}(t^*)$ decays for all time when we choose $c(X) = 1$ and apply the control law (4.6) with $\gamma > 1$.

Case 2. For boundary conditions given by

$$A(0,t^*)=A_{XX}(0,t^*)=0 \quad \text{and} \quad A(1,t^*)=0 \quad \text{for } t^*>0, \tag{4.10}$$

the energy $\tilde{E}(t^*)$ decays for all time when we choose $c(X)=1-X$ and apply the control law (4.6) with $\gamma>1$.

Case 3. For boundary conditions given by

$$A(0,t^*)=A_{XX}(0,t^*)=0 \quad \text{and} \quad c_1A_X(1,t^*)+c_2A(1,t^*)=0 \quad \text{for } t^*>0, \tag{4.11}$$

with $c_1>0, c_2>0$ and $c_1+c_2=1$, the energy $\hat{E}(t^*)$ decays for all time when we choose $c(X)=1-c_2X$ and apply the control law (4.6) with $\gamma>1$.

Note that the same control law for $u(t^*)$ is used in the three cases with various outlet conditions. The first case is applicable to long pipes. The second case may represent a fixed flux condition at the outlet of a finite-length pipe. The third case may fit to a wide range of physical situations with various outlet devices. The only difference is the axial profile function $c(X)$ adapted in each case.

In the proposed control law (4.6), we relate at all time the control command $u(t^*)$ to the negative of the inlet radial velocity at an off-centre position. Note that the inlet radial velocity is the major source for the production of perturbation's kinetic energy associated with the axial velocity perturbation and dominates the growth of the perturbation, see Wang & Rusak (2011) for a detailed discussion of the perturbation's energy production mechanism. The analysis according to the long-wave (long-pipe) model (4.1) shows that by actively feeding back a control command that is related at all time to the opposite sign of the evolving inlet radial velocity, the control action opposes the gain of energy at the inlet, dissipates the energy and reduces the production of perturbation's kinetic energy $\tilde{E}$ and its total kinetic energy, thereby forcing the perturbation to decay in time.

4.2. *Conditions on the control gain γ according to the long-wave dynamics*

We consider the role of the control gain γ. The main result from the analysis below is that excessive control with large γ does not necessarily lead to an effective control. On the contrary, we show that either the borderline case where $\gamma=1$ (or close to 1) or the case where γ is sufficiently large lead to control with zero (or close to zero) growth rate of the stability modes. Such a control suffers a narrow margin of controllability that may be lost when pipe length is not necessary long or when nonlinear effects are also considered.

We consider the problem (4.1) with (4.6). Let $A(X,t^*)=\tilde{A}e^{\sigma^* t^*}$ and $u(t^*)=-2\kappa_\omega\gamma\tilde{A}_X(0)e^{\sigma^* t^*}$. Inserting it into (4.1), one obtains an eigenvalue problem for Case 1 (where $c(X)=1$):

$$2\Omega_B\sigma^*\tilde{A}=\tilde{A}_{XXX}+4\kappa_\omega\tilde{A}_X-2\kappa_\omega\gamma\tilde{A}_X(0) \quad \text{for } 0\leqslant X\leqslant 1, \tag{4.12a}$$

$$\tilde{A}(0)=\tilde{A}_{XX}(0)=\tilde{A}_X(1)=0. \tag{4.12b}$$

We consider the situation where a neutral mode with $\sigma^*=0$ exists when $\kappa_\omega>0$. This case poses a limit on the feedback control effectiveness. With $\sigma^*=0$, the eigenvalue problem reduces to

$$\tilde{A}_{XXX}+4\kappa_\omega\tilde{A}_X=2\kappa_\omega\gamma\tilde{A}_X(0) \quad \text{for } 0\leqslant X\leqslant 1, \tag{4.13a}$$

$$\tilde{A}(0)=\tilde{A}_{XX}(0)=\tilde{A}_X(1)=0, \tag{4.13b}$$

which can be solved analytically. Assuming that $\tilde{A}_X(0)=1$ (a scaling parameter of the linear problem) we find that $\tilde{A}(X)=\gamma X/2$ solves the non-homogeneous

problem (4.13). Also, the homogeneous problem of (4.13) has a characteristic solution $\tilde{A} = e^{aX}$ where a is found from the roots of

$$a^3 + 4\kappa_\omega a = 0. \tag{4.14}$$

The solutions of (4.14) are $a_1 = 0$ and $a_{2,3} = \pm 2\sqrt{\kappa_\omega} i$. The general solution for (4.13) is given by the linear combination:

$$\tilde{A}(X) = C_1 \sin(2\sqrt{\kappa_\omega} X) + C_2 \cos(2\sqrt{\kappa_\omega} X) + C_3 + \tfrac{1}{2}\gamma X. \tag{4.15}$$

From conditions $\tilde{A}(0) = 0$ and $\tilde{A}_{XX}(0) = 0$, one obtains $C_2 = 0$ and $C_3 = 0$, and

$$\tilde{A}(X) = C_1 \sin(2\sqrt{\kappa_\omega} X) + \tfrac{1}{2}\gamma X. \tag{4.16}$$

The coefficient C_1 is determined from $\tilde{A}_X(1) = 0$ and $\tilde{A}_X(0) = 1$ (as assumed); we have

$$2C_1\sqrt{\kappa_\omega} + \tfrac{1}{2}\gamma = 1 \quad \text{and} \tag{4.17}$$

$$2C_1\sqrt{\kappa_\omega}\cos(2\sqrt{\kappa_\omega}) + \tfrac{1}{2}\gamma = 0. \tag{4.18}$$

Then, the necessary and sufficient conditions for the solution of (4.17) and (4.18) are given by

$$\cos(2\sqrt{\kappa_\omega}) = \frac{\gamma}{\gamma - 2}. \tag{4.19}$$

The necessary and sufficient conditions for the existence of a neutral mode of (4.12) are

$$\left| \frac{\gamma}{\gamma - 2} \right| \leqslant 1. \tag{4.20}$$

It can be concluded from (4.20) that when $\gamma < 1$, the growth rate must change its sign at various swirl ratios and the flow becomes uncontrollable. When $\gamma = 1$, we have $\gamma/(\gamma - 2) = -1$ and there exist infinitely many neutral modes at various swirl ratios. Thus, the control with $\gamma = 1$ is indeed at the borderline of applicability of the control method. When $\gamma > 1$ (as required by the control law), (4.19) has no solution and control is achieved. However, when control gain $\gamma \gg 1$, the effectiveness of the feedback stabilization is reduced. In fact, $\gamma/(\gamma - 2) \to 1$ as $\gamma \to \infty$ and this leads to the existence of near neutral modes of the eigenvalue problem (4.12) and a marginal control. Finally, we observe that $\gamma = 2$ is the only singular point of $\gamma/(\gamma - 2)$ and no solution of (4.19) exists. In this sense, $\gamma = 2$ is a possibly best gain for the feedback control. This result is useful for applying the proposed control method. We demonstrate in § 4.4 that this is indeed the case, where the control effectiveness is assessed in terms of the growth rate according to the full controlled linear dynamics. Xu (2012) found from a numerical study using the long-wave model for a Lamb–Ossen vortex that the gain $\gamma = 2$ gives the fastest decay of perturbations.

In the following section we use the control strategy developed here in the full linear dynamics problem for case 1 and assess the effectiveness of the proposed control method.

4.3. *The control of the solid-body rotation flow using the full linear dynamics*

The control approach developed in § 4.1 and § 4.2 based on the long-wave problem is used now in the full linear dynamics problem (3.16). Here, we replace the fixed circulation profile at the inlet and consider it to be time varying in the form

$$K(0, t^*) = 2\omega y + \epsilon \phi_B(y) k(t^*), \tag{4.21}$$

where $0 < |\epsilon| \ll 1$ and $k(t^*)$ is the control command in time. From the basic linearized governing (3.2), we find that

$$2\omega K_{1t} = -2y(\chi_{1t} + \chi_{1x}) + 4\omega^2 \psi_{1x}. \tag{4.22}$$

Note that at the inlet $K_{1t^*}(0, t^*) = \phi_B(y) k_{t^*}(t^*)$. At the inlet $X = 0$, equation (4.22) becomes

$$2\omega k_{t^*}(t^*) = \left(\mathscr{A}_{XXX}(0, t^*) + \left(4\kappa_\omega + \frac{4\kappa_\omega^2 \epsilon_1}{\Omega_B} \right) \mathscr{A}_X(0, t^*) \right). \tag{4.23}$$

The mathematical problem (3.16), after being modified with the circulation control at the inlet defined by (4.21), takes the form

$$\mathscr{A}_{XXXX} - 2\Omega_B \mathscr{A}_{Xt^*} + 4\kappa_\omega \mathscr{A}_{XX} + 2\epsilon_1 \mathscr{A}_{XXXt^*} + \frac{4\kappa_\omega^2 \epsilon_1}{\Omega_B} \mathscr{A}_{XX} + \epsilon_1^2 \mathscr{A}_{XXt^*t^*} - \epsilon_1 \Omega_B \mathscr{A}_{t^*t^*} = 0. \tag{4.24a}$$

$$\mathscr{A}(0, t^*) = \mathscr{A}_{XX}(0, t^*) = 0, \tag{4.24b}$$

$$\mathscr{A}_{XXX}(0, t^*) + \left(4\kappa_\omega + \frac{4\kappa_\omega^2 \epsilon_1}{\Omega_B} \right) \mathscr{A}_X(0, t^*) = 2\omega k_{t^*}(t^*) \quad \text{and} \quad \mathscr{A}_X(1, t^*) = 0. \tag{4.24c}$$

For the case of a long pipe $\epsilon_1 = 1/L^2 \sim 0$ and $\omega \sim \omega_B$, the terms in the second line of (4.24*a*) are of the order ϵ_1 or higher, and may be neglected. Then integrating it with respect to X and using the boundary conditions in (4.24*b*) and (4.24*c*) yields

$$\mathscr{A}_{XXX} - 2\Omega_B \mathscr{A}_{t^*} + 4\kappa_\omega \mathscr{A}_X - 2\omega k_{t^*}(t^*) = 0, \tag{4.25a}$$

$$\mathscr{A}(0, t^*) = 0, \quad \mathscr{A}_{XX}(0, t^*) = 0 \quad \text{and} \quad \mathscr{A}_X(1, t^*) = 0. \tag{4.25b}$$

Comparing (4.25) with (4.1), we find that the control term $u(t^*)$ can be realized by swirl control $u(t^*) = -2\omega k_{t^*}(t^*)$. This leads to the control law for $k(t^*)$ as

$$2\omega k_{t^*}(t^*) = 2\gamma \kappa_\omega A_X(0, t^*) \quad \text{with } \gamma \geqslant 1. \tag{4.26}$$

It is anticipated that the perturbation on the solid-body rotation flow as described by the full linear dynamics problem can be as well controlled by the inlet swirl control law (4.26) for ω sufficiently close to ω_B. However, when ω is beyond the initial range where the long-wave approach is valid, it is not clear that the full linear dynamics problem can be still stabilized by the proposed feedback methodology (4.26). Further investigation is needed.

It is more suitable to use the following control law

$$2\omega k_{t^*}(t^*) = \frac{\gamma}{2} \frac{\Omega - \Omega_B}{\epsilon_1} \mathscr{A}_X(0, t^*), \quad \gamma \geqslant 1, \tag{4.27}$$

for the full linear dynamics problem, which is equivalent to (4.26) at the long pipe limit since $(\Omega - \Omega_B)/\epsilon_1 \sim 4\kappa_\omega$ for a long pipe. Introducing the mode analysis $\mathscr{A}(X, t^*) = \tilde{\mathscr{A}}(X) \mathrm{e}^{\sigma^* t^*}$ into (4.24), one obtains an eigenvalue problem,

$$\tilde{\mathscr{A}}_{XXXX} + \frac{\Omega - \Omega_B}{\epsilon_1} \tilde{\mathscr{A}}_{XX} - 2\Omega_B \sigma^* \tilde{\mathscr{A}}_X + 2\epsilon_1 \sigma^* \tilde{\mathscr{A}}_{XXX} + \epsilon_1^2 \sigma^{*2} \tilde{\mathscr{A}}_{XX} - \epsilon_1 \Omega_B \sigma^{*2} \tilde{\mathscr{A}} = 0, \tag{4.28a}$$

$$\tilde{\mathscr{A}}(0) = 0, \quad \tilde{\mathscr{A}}_{XX}(0) = 0, \quad \tilde{\mathscr{A}}_{XXX}(0) + \frac{\Omega - \Omega_B}{\epsilon_1} \tilde{\mathscr{A}}_X(0) = \frac{\gamma}{2} \frac{\Omega - \Omega_B}{\epsilon_1} \tilde{\mathscr{A}}_X(0) \quad \text{and} \quad \tilde{\mathscr{A}}_X(1) = 0. \tag{4.28b}$$

The relationship $4\kappa_\omega+4\kappa_\omega^2\epsilon_1/\Omega_B=(\Omega-\Omega_B)/\epsilon_1$ was used here. The flow controllability requires that the real parts of the eigenvalues σ^* of (4.28) are all non-positive.

We rigourously prove in appendix B the following energy identity:

$$\frac{1}{2}\tilde{\mathscr{A}}_{XX}^2(1)+\frac{1}{2}(\gamma-1)\frac{\Omega-\Omega_B}{\epsilon_1}\tilde{\mathscr{A}}_X^2(0)+\frac{1}{2}\epsilon_1^2\sigma^{*2}\tilde{\mathscr{A}}_X^2(0)+\frac{1}{2}\epsilon_1\Omega_B\sigma^{*2}\tilde{\mathscr{A}}^2(1)$$
$$=-\sigma^*\int_0^1(2\Omega_B\tilde{\mathscr{A}}_X^2+2\epsilon_1\tilde{\mathscr{A}}_{XX}^2)\,\mathrm{d}X. \tag{4.29}$$

For stability modes of full linear control problem (4.28) with real eigenmodes and growth rates σ^*, the left-hand side of (4.29) is non-positive. Thus, we obtain the following fundamental result for the feedback control law of the full linear control problem:

> When eigenvalues σ^* of problem (4.28) are real, they are always negative when the control gain $\gamma>1$.

Note that the last two terms in the left-hand side of (4.29), which are neglected in the weakly nonlinear long-wave model, are non-negative and thus have a stabilizing effect on the flow.

It is natural to ask whether or not the same conclusion can be drawn for the complex σ^*. The answer is in general negative. The complication arises from the terms in the left-hand side of (4.29) with σ^{*2}, whose real component may become negative for σ^* complex. The numerical computations in § 4.4 show that the real component of the complex growth rate branches can indeed become positive for some control gain γ in a range of swirl ratio. In physics, this means that the perturbations have more complicated behaviour due to the appearance of conjugate complex eigenmodes, which arise as a consequence of the merging of two real eigenmodes at specific swirls.

4.4. *The linear growth rate according to the full linear control problem (4.28)*

The linear stability problem (4.28) using the full linear controlled dynamics is solved by a standard shooting method. We conducted a thorough computation of the growth rates for a flow in a pipe with $L=6$ for various control gains γ and in a swirl range $\sim$50 % above the first critical swirl $\omega_1=1.920$. The results confirm all of the theoretical predictions developed in the previous sections, and reveal explicitly the complicated behaviour of the feedback stabilization method.

Figure 2 shows the growth rates with control gains $\gamma=1.9$, $\gamma=2$ and $\gamma=2.4$, respectively, for the swirl range up to $\omega=3$. All of the growth rates have negative real parts, which shows the decay of all perturbation modes of the full linear control problem in the whole range of swirl, where the flow is unstable in the natural dynamics without flow control, see figures 1 and 2. It is found that the real growth rate branches in all of the cases computed are negative as predicted by the theory, and their values are seen to be progressively decreasing along with the increase of the swirl. One notices that the decrease of the real branches with $\gamma=2$ is the fastest among the cases, indicating best performance of the feedback control with this gain. Note from (4.28) that for the control with gain $\gamma=2$ we actually control $\tilde{\mathscr{A}}_{XXX}(0)=0$ in addition to $\tilde{\mathscr{A}}(0)=0$ and $\tilde{\mathscr{A}}_{XX}(0)=0$, which is a special physical mechanism of control.

All branches of complex growth rates bifurcate from the fold points of the real growth rate branches. The real parts of the complex growth rates stay nearly constant but oscillate with swirl. As shown, for example, for the case $\gamma=2$, the value of the real part of the least stable complex growth rate branch is oscillating in the range

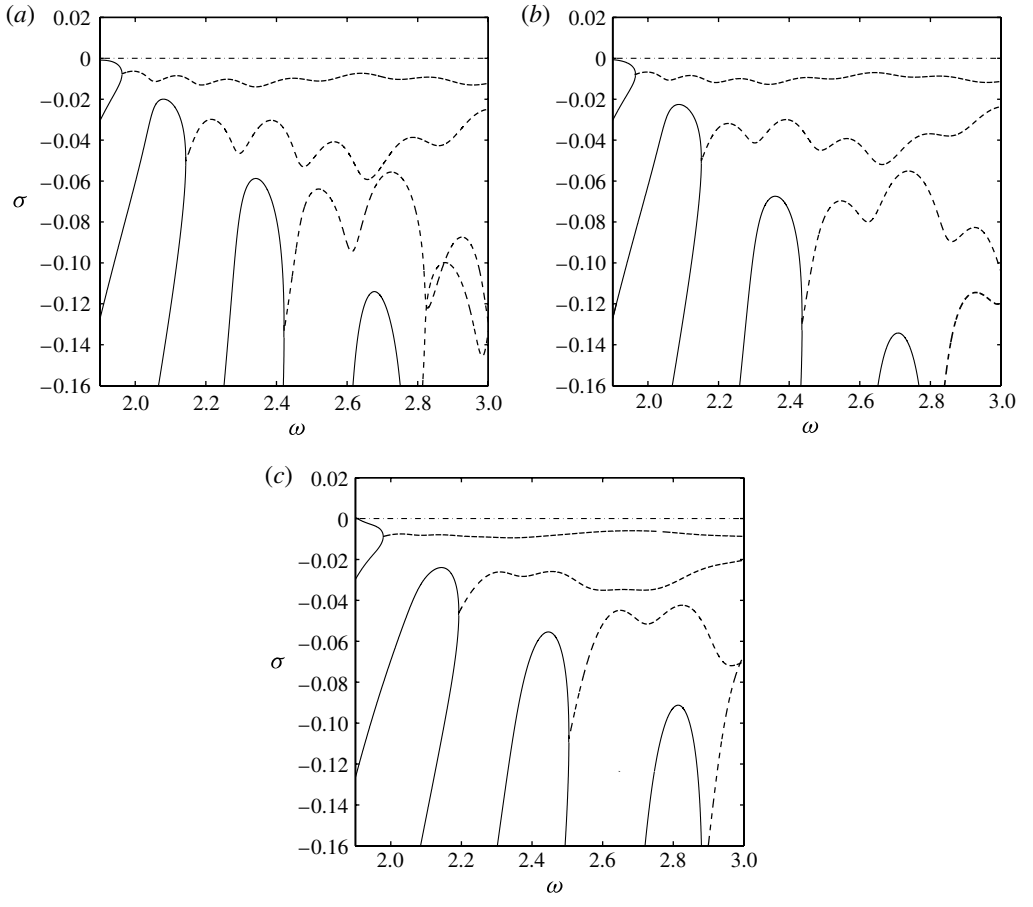

FIGURE 2. The growth rate σ versus the swirl parameter ω. The solid line indicates the real growth rate branches and the dotted line indicates the complex growth rate branches: (*a*) $\gamma = 1.9$; (*b*) $\gamma = 2$; (*c*) $\gamma = 2.4$.

between -0.0068 and -0.0095. The other complex growth rate branches oscillate in the range of more negative values. Results indicate that flow stabilization can also be achieved for a swirl ratio above $\omega = 3$.

Figure 3 shows the growth rates with control gains $\gamma = 1$ and $\gamma = 10$, respectively, for the swirl range up to $\omega = 3$. These are two typical cases with inadequate amount of feedback gain for the control, either insufficient or excessive. It is found that the real growth rate branches in either case are indeed non-positive as predicted by the theory, but their peak value at each branch is either zero ($\gamma = 1$) or close to zero ($\gamma = 10$).

All branches of complex growth rates bifurcate from the fold points of the real growth rate branches. The real parts of the complex growth rates become positive at certain swirl ratios. This means instability modes develop and feedback stabilization is lost in both cases. The long-wave control approach which predicts controllability for every $\omega > \omega_B$ with $\gamma > 1$ is actually valid only when swirl ratio is slightly above ω_B up to $\omega = 2.11$ when $\gamma = 1$ and up to $\omega = 2.4$ when $\gamma = 10$. This is in sharp contrast to the case with γ around 2.

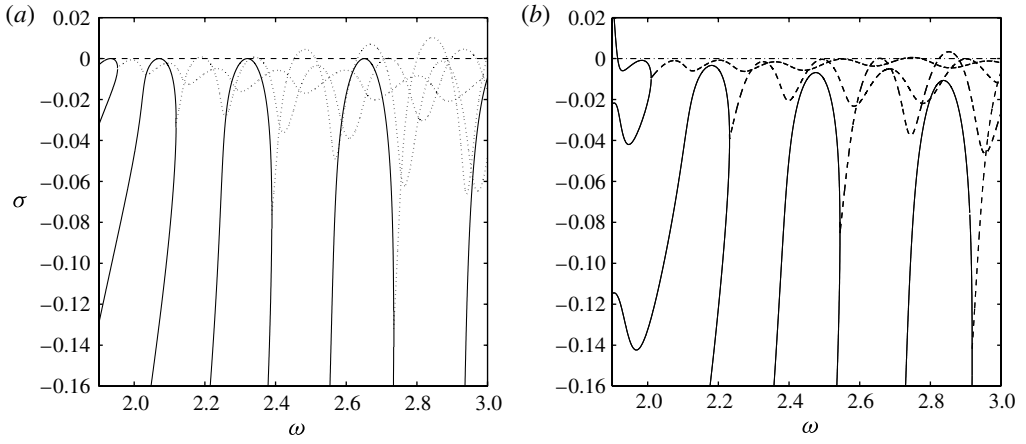

FIGURE 3. The growth rate σ versus the swirl parameter ω. The solid line indicates the real growth rate branches and the dotted line indicates the the complex growth rate branches: (*a*) $\gamma = 1$; (*b*) $\gamma = 10$.

The stability modes according to the full linear control problem shows the control effectiveness is sensitive to the choice of the feedback control gain. The range gain of γ around 2 ($1.5 < \gamma < 2.5$) gives the fastest decay of the perturbation for a wide range of swirl. However, insufficient or excessive gains lead to failure of the control method as the swirl is increased.

At this point, we would like to clarify the difference between Gallaire *et al.* (2004) control method and the present feedback stabilization method. Gallaire *et al.* (2004) used the linear perturbation equations together with linear optimal control theory to minimize a cost function that is based on the perturbation size and the control power and to derive their feedback control rule. Their control method requires measurement of the perturbation in the whole domain which is not easy to realize. Also, it is limited to a relatively small range of swirl up to 7 % above ω_1. On the other hand, we use a perturbation energy identities (4.4) and (4.5), with no limit of control power, to reveal a relatively robust feedback control law (4.6) that requires only a single measurement of the radial velocity at an off centreline point at the inlet. Our control approach with gain γ around 2 suppresses all natural instability modes up to 50 % above ω_1, and even more can be achieved.

4.5. *The stability mode shapes and control mechanism according to the full linear problem*

In this section we shed additional light on the physical mechanism of the proposed feedback control method. We first consider the eigenmodes of the full linear control problem (4.28) for various control gains γ and their physical implications. We focus on the swirl range near ω_B. Figure 4(*a*) shows only the least-stable branches of the growth rate curves for $\gamma = 1$, 2 and 10, respectively. They are all real growth rate branches. For $\gamma = 1$ and 10 the curve has a maximum point with negative value near 0. Also, each of the curves exhibits a fold point from which complex eigenvalues bifurcate (see § 4.4).

Figure 4(*b*) shows six eigenmodes for swirl ratios equally space in the range $1.934 \leqslant \omega \leqslant 1.952$. For the case $\gamma = 1$, figure 4(*c*) shows six eigenmodes for swirl ratios equally space in the range $1.940 \leqslant \omega \leqslant 1.963$. For the case $\gamma = 10$, figure 4(*d*) shows six eigenmodes for swirl ratios equally space in the range $1.985 \leqslant \omega \leqslant 2.008$.

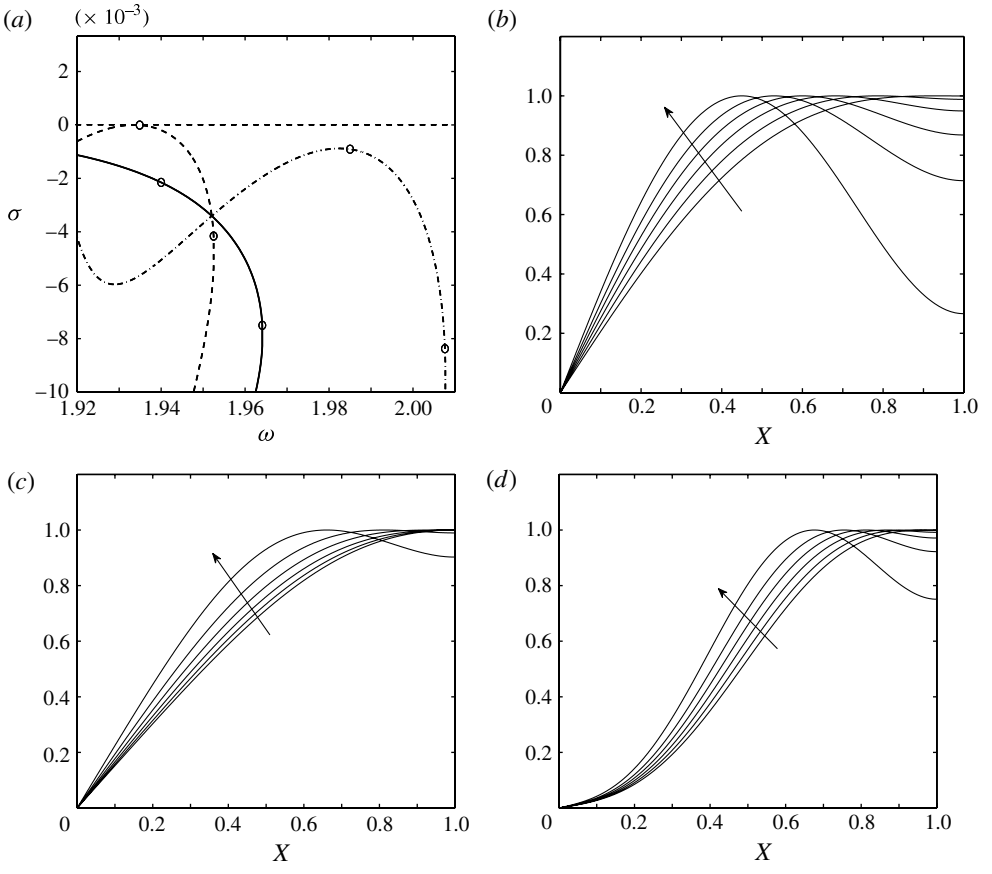

FIGURE 4. (*a*) The growth rate σ versus the swirl ω: the dashed line is the case $\gamma = 1$, the solid line is $\gamma = 2$ and the dashed dotted line is $\gamma = 10$. (*b*) Six eigenmodes for the case $\gamma = 1$ (between the two open circles marked on the growth rate curve). (*c*) and (*d*) Similar plots for the cases $\gamma = 2$ and 10, respectively. The arrow points to the increase of the swirl.

In these figures the linear mode shape functions $\tilde{\mathscr{A}}(X)$ are rescaled such that their maximum value is 1. It can be seen that the mode shapes are affected by the control gain γ and thereby they influence the control effectiveness. For $\gamma = 1$, the feedback gain is at the borderline of control. The resulting eigenmodes change shape from near $\sin(\pi X/2)$ at $\omega = 1.934$ to waves with greater relative slopes at the pipe inlet as the swirl ratio approaches the fold point at $\omega = 1.952$. This indicates that the control gain $\gamma = 1$ induces relatively large inlet radial velocity perturbations which are not sufficiently suppressed. They may even grow out of control due to nonlinear effects.

For $\gamma = 2$, the resulting eigenmodes in the range $\omega = 1.940$ to $\omega = 1.963$ (the fold point) are overall similar to those for the case $\gamma = 1$ but with smaller relative slopes at the inlet. This allows a relatively effective feedback control of the perturbations since a moderate control gain induces relatively moderate inlet radial velocity perturbations that are sufficiently suppressed.

When feedback gain is increased to $\gamma = 10$, the relative slopes of the eigenmodes at the inlet decrease significantly with respect to the cases with $\gamma = 1$ and 2. This reveals a different physical mechanism of the feedback control with a large gain γ.

The control $\gamma = 10$ is directly related to the suppression of the radial velocity perturbation at the pipe inlet, i.e. the feedback control is based on the inlet radial velocity perturbation and with a too large gain it results in a too small inlet radial velocity perturbation and, thereby, reduces the effectiveness of the feedback control.

In summary, the eigenmode slope at the inlet provides insight into the control mechanism. When the slope is too large, the response of the flow to control command is too soft to force the perturbation decay. On the other hand, when the inlet slope is too small flow response to the control command is too stiff, therefore not so effective.

To complete the discussion, we provide additional quantitative analysis of the energy identity (4.29). From (4.29) we find that the damping mechanism in the feedback control is mainly contributed by the two terms on the left-hand side of this equation; the first term, $\tilde{\mathscr{A}}_{XX}^2(1)/2$, reflects the stabilizing role of the dispersion of perturbations and the second term, $(\gamma - 1)((\Omega - \Omega_B)/\epsilon_1)\tilde{\mathscr{A}}_X^2(0)/2$, reflects the suppression of the radial velocity perturbation at the pipe inlet by the feedback control when $\omega > \omega_B$. The other two terms on the left-hand side of (4.29) are of higher order and may be neglected when ϵ_1 is sufficiently small. For $\gamma = 1$, the second term on the left-hand side of (4.29) vanishes and the perturbation's damping mechanism is primarily from the first term on the left-hand side of (4.29). For the feedback gain $\gamma > 1$, we calculate the contributions of the two leading terms in (4.29) to the growth rate by splitting σ into two respective growth rates,

$$\sigma = \sigma_1 + \sigma_2 + O(\epsilon_1), \tag{4.30a}$$

$$\sigma_1 = -\epsilon_1^{3/2}\frac{\tilde{\mathscr{A}}_{XX}^2(1)}{2I}, \tag{4.30b}$$

$$\sigma_2 = -\epsilon_1^{1/2}(\gamma - 1)\frac{\Omega - \Omega_B}{2I}\tilde{\mathscr{A}}_X^2(0). \tag{4.30c}$$

Here

$$I = \int_0^1 (2\Omega_B\tilde{\mathscr{A}}_X^2 + 2\epsilon_1\tilde{\mathscr{A}}_{XX}^2)\,\mathrm{d}X. \tag{4.31}$$

The computations of σ_1 and σ_2 and their comparisons with σ for $\gamma = 2$ and 10 are shown in figure 5(*a*,*b*), respectively.

For $\gamma = 2$, the second term on the left-hand side of (4.29) has a significant role in the perturbation's damping mechanism. As shown in figure 5(*a*) the growth rate curve of σ is closely followed by the σ_2 curve while σ_1 is much smaller. One notices that for this case both $(\gamma - 1)$ and $\tilde{\mathscr{A}}_X^2(0)$ retain an order $O(1)$ and dominate the growth rates and its eigenmode. Thereby, the feedback control with $\gamma = 2$ is strongly engaged in the mechanism of suppression of perturbations.

For $\gamma = 10$, the excessive feedback strongly suppresses the development of the radial perturbation at the inlet, resulting in a mode shape with much smaller slope at the inlet $X = 0$. Then, the term $\tilde{\mathscr{A}}_X^2(0)$ becomes much smaller. This substantially reduces the damping effect from the second term on the left-hand side of (4.29). As shown in figure 5(*b*), the growth rate curve of σ is now closely followed by σ_1 curve whereas σ_2 is much smaller. It is clear that when γ increases above 2, the radial velocity perturbation decreases and the overall contribution from the feedback control term to the suppression of the perturbations is reduced. In physical situations, the feedback control with large gains γ appears to be too stiff, while the control with gain $\gamma = 2$ is more flexible and thus more effective.

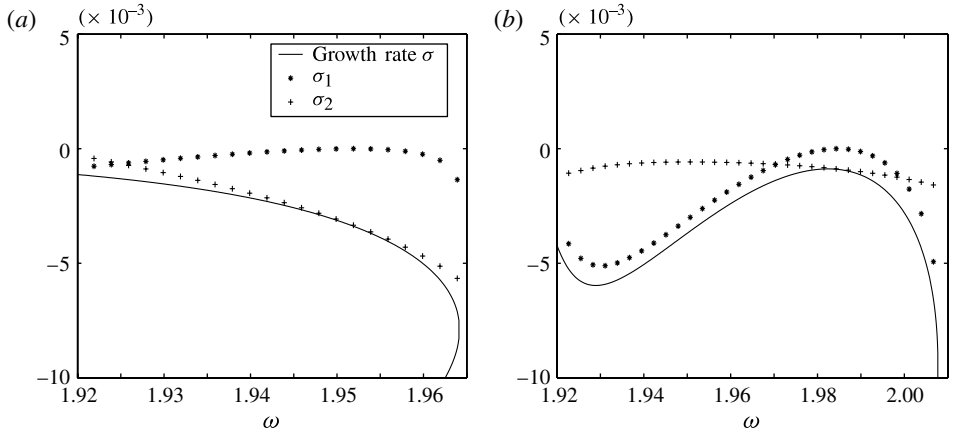

FIGURE 5. The contributions to the damping mechanism: . (*a*) the case $\gamma = 2$ and (*b*) the case $\gamma = 10$. The star symbols ($*$) show σ_1 and the plus symbols ($+$) show σ_2.

4.6. *The response of the control approach to inlet flow perturbations according to the long-wave linear problem*

We study the robustness of the proposed control method to inlet flow perturbations. We use the long-wave (long-pipe) linear problem (4.25) and redefine $k(t^*)$ as $k_0 \sin(2\pi f t^*) + k(t^*)$. The first term represents inlet sinusoidal circulation perturbations with amplitude k_0 and frequency f and the second term the active control command. Substituting this into (4.25) we obtain the problem

$$\mathscr{A}_{XXX} - 2\Omega_B \mathscr{A}_{t^*} + 4\kappa_\omega \mathscr{A}_X - 4\pi f \omega \cos(2\pi f t^*) - 2\omega k_{t^*}(t^*) = 0, \tag{4.32a}$$

$$\mathscr{A}(0, t^*) = 0, \quad \mathscr{A}_{XX}(0, t^*) = 0 \quad \text{and} \quad \mathscr{A}_X(1, t^*) = 0. \tag{4.32b}$$

An initial perturbation is also considered in the form of a representative wave, $\mathscr{A}(X, 0) = \delta \sin(\pi X/2)$. Here δ represents the size of the initial perturbation.

The solution of this linear problem is composed of a linear combination of the solution to the control problem (4.32) with an initial perturbation size $\delta = -1$ and with no inlet flow perturbation ($k_0 = 0$) and the solution of the control problem (4.32) with no initial perturbation ($\delta = 0$) and with a continuous inlet flow perturbation with $k_0 = 1$ and $f = 1$. The active feedback control law (4.26) with $\gamma = 2$ is used for each of these solutions. The problem (4.32) is solved numerically using a two-step temporal integration method and central finite differences in X (see the details of the technique in Rusak *et al.* 2012). In the following computed examples we focus on the representative case where the incoming swirl is $\omega = 1.95$ and the pipe non-dimensional length is $L = 6$ (or $\epsilon_1 = 1/36$).

The natural evolution of the flow perturbation mode $\mathscr{A}(t^*)$ in the two cases with no control ($\gamma = 0$) is first computed. Figure 6 presents the evolution of the mode minimum ($\mathscr{A}_{min}$, the solid line), maximum ($\mathscr{A}_{max}$, the dotted line) and outlet ($\mathscr{A}_{out}$, the dashed line) values. Figure 6(*a*) is for the case with $\delta = -1$ (an initial deceleration wave) and $k_0 = 0$ and figure 6(*b*) is for the case with $\delta = 0$ and $k_0 = 1$, $f = 1$. Figure 6(*a*) shows that the initial wave first reshapes during the transient period $0 < t^* < 0.5$ to the unstable mode at $\omega = 1.95$ and then grows in size with a constant growth rate $\sigma^* = 0.78$ and a fixed shape, showing increasing deceleration along the pipe centreline with time. This is the initiation of the vortex breakdown process induced by an initial deceleration wave. Figure 6(*b*) shows the flow response to

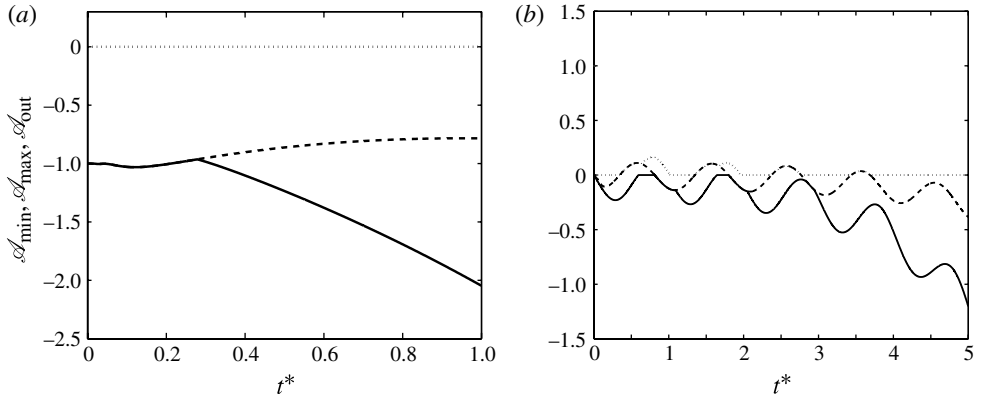

FIGURE 6. The natural ($\gamma = 0$) evolution of the mode minimum (solid line), maximum (dotted line) and outlet (dashed line) values at $\omega = 1.95$ for the cases: (*a*) $\delta = -1$ and $k_0 = 0$; (*b*) $\delta = 0$, $k_0 = 1$ and $f = 1$.

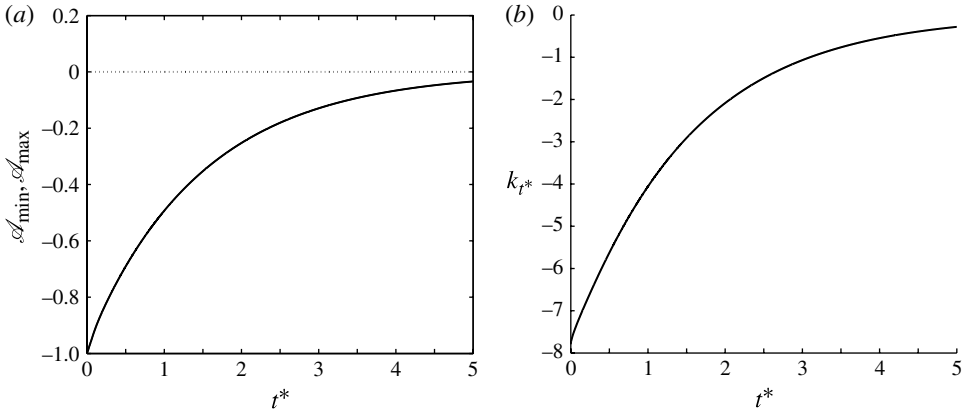

FIGURE 7. The feedback controlled evolution at $\omega = 1.95$ with $\gamma = 2$ of the perturbation mode: (*a*) the mode minimum (solid line), maximum (dotted line) and outlet (dashed line) values for the case $\delta = -1$ and $k_0 = 0$; (*b*) the evolution of the controller k_{t^*}.

the continuous inlet sinusoidal perturbation. Again, the mode first reshapes during the transient period $0 < t^* < 3$ and then grows exponentially with oscillations with frequency 1 and with increasing deceleration perturbations along the pipe centreline. This is the initiation of the vortex breakdown process but now induced by a continuous inlet flow perturbation.

The controlled evolution of the flow perturbation mode in the case with $\delta = -1$, $k_0 = 0$ is shown in figure 7. The exponential decay in time of the perturbation mode minimum, maximum and outlet values and of the controller k_{t^*} is evident from figure 7(*a*,*b*), respectively. The decay rate is constant, $\sigma^* = -0.68$. The controller is able to cut the feed-forward natural growth of the initial wave (as shown in figure 6*a*) and enforce a decay of the perturbation within $t^* < 5$ and a return of the swirling flow to a columnar state. This demonstrates the elimination of the breakdown process induced by the initial wave as long as the controller is active.

The controlled evolution of the flow perturbation mode in the case with $\delta = 0$, $k_0 = 1$ and $f = 1$ is shown in figure 8. The perturbation mode minimum, maximum and

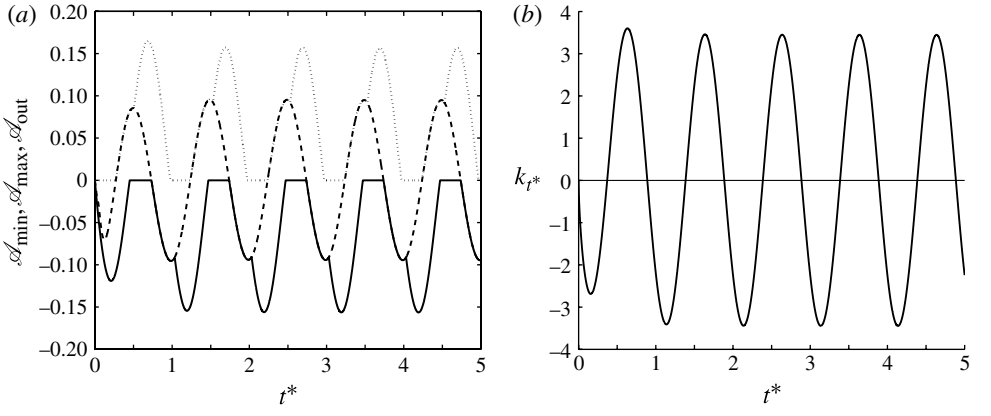

FIGURE 8. The feedback controlled evolution at $\omega = 1.95$ with $\gamma = 2$ of the perturbation mode: (*a*) the mode minimum (solid line), maximum (dotted line) and outlet (dashed line) values for the case $\delta = 0$ and $k_0 = 1, f = 1$; (*b*) the evolution of the controller k_{t^*}.

outlet values and the controller k_{t^*} exhibit, after a short transient stage, a sinusoidal response with no growth or decay, see figure 8(*a*,*b*), respectively. The controller is able to cut the natural growth of the perturbation mode in response to the continuous inlet perturbation (as shown in figure 6*b*) and to enforce a bounded sinusoidal response of the perturbation when $t^* > 3$ with frequency 1 as imposed at the inlet. This demonstrates the robustness of the control law (4.26) with $\gamma = 2$ to stabilize continuous inlet flow perturbations.

Finally, the controlled evolution of the flow perturbation mode in the combined case with $\delta = -1$, $k_0 = 1$ and $f = 1$ is shown in figure 9. The solution is a linear combination of the solutions presented in figures 7 and 8. The perturbation mode minimum, maximum and outlet values and the controller k_{t^*} first decay over the time period $0 < t^* < 3$ as a result of the imposed decay of initial wave by the controller. Then, the perturbation mode and the controller are dominated by the sinusoidal response with no growth or decay, see figure 9(*a*,*b*), respectively. This demonstrates again the ability of the control law (4.26) with $\gamma = 2$ to overcome the growth of both the initial wave and the continuous inlet flow perturbation, stabilize the base flow, and eliminate the vortex breakdown process.

5. Conclusions and discussion

The theoretical foundation and the physical mechanisms of a newly proposed feedback-stabilization method of a vortex flow in a finite-length, straight circular pipe are established. In the natural dynamics without control, linearly unstable modes appear in sequence as swirl ratio ω is increased beyond the critical level ω_1 (see figure 1). For an effective stabilization of the base vortex flow, all of the unstable perturbation modes must be eliminated by applying a suitable control law. We formulate a new active control method from an extended perturbation's kinetic energy analysis that is based on the long-wave (long-pipe) model. Information about the inlet radial velocity is actively fed back to the controller, multiplied by a gain γ, and globally suppresses the perturbation's kinetic energy and thereby quenches all of the unstable modes of the flow when $\omega > \omega_1$. We prove that the feedback control methodology can be applied to various physical settings at the pipe inlet and outlet

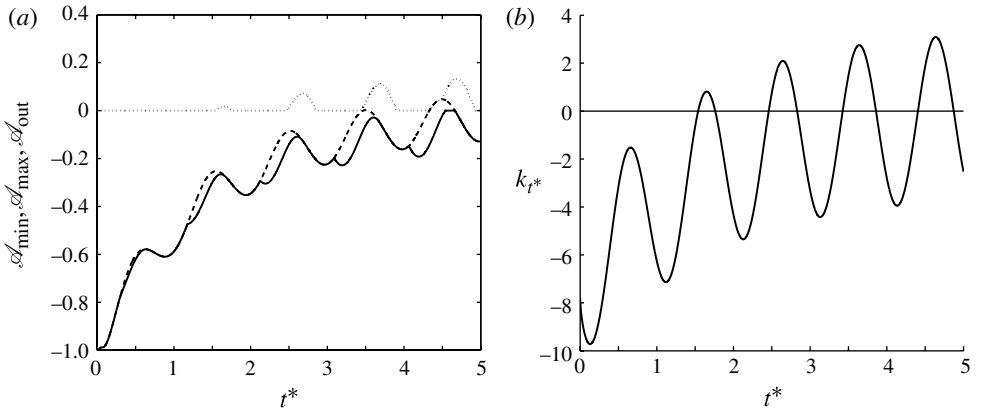

FIGURE 9. The feedback controlled evolution at $\omega = 1.95$ with $\gamma = 2$ of the perturbation mode: (*a*) the mode minimum (solid line), maximum (dotted line) and outlet (dashed line) values for the case $\delta = -1$ and $k_0 = 1, f = 1$; (*b*) the evolution of the controller k_{t^*}.

boundaries. Essentially, this active control strategy cuts the feed-forward mechanism between the inlet radial velocity and the growth of perturbations in the bulk revealed by Wang & Rusak (2011) and eliminates the breakdown process. This analysis also emphasizes the importance of the long-wave model of Rusak *et al.* (2012) as a fundamental tool for clearly elucidating the major physical mechanisms leading to vortex breakdown and for revealing the effective method of the vortex flow control.

Through a neutral stability analysis of the long-wave linear feedback control problem, we prove that either too small control gain (γ is greater but close to 1) or excessive control gain ($\gamma \gg 1$) may lead to nearly neutral modes and marginal flow control. We also find that the control gain $\gamma = 2$ may provide the most effective control since for this gain all of the modes of the long-wave linear control problem are far from neutral and stable. This indicates the need for correctly identifying a range of effective control gains to ensure flow stabilization for a wide range of swirl ratios.

To further access the applicability and properties of the proposed control methodology at various swirl ratios and control gains, we apply it to the full linear control problem for a swirling flow with any swirl ratio in a finite-length pipe that is not necessarily long. We focus on the case where the base state is given by a solid-body rotation flow. This case offers analytical simplicity and important insight into the control strategy. We analytically derive the novel energy identity (4.29) for the full linear control problem which connects the growth rate of the controlled flow stability modes to the specific damping mechanisms prompted by the feedback control. Using this energy identity, we establish that all stability modes of the full linear control problem that have real growth rates are stable (growth rates are negative). Our computations in figures 2 and 3 show that the complex eigenmodes of the full linear control problem bifurcate from fold points of branches of modes with real growth rates and are also stable within a range of swirl near the fold swirl level. However, explicit examples show that the complex eigenmodes can become unstable (the real part of growth rate becomes positive) when swirl is further increased and certain inadequate control gains γ are used; when γ is around 1 or $\gamma \gg 1$ (see figure 3). When $\gamma = 2$ or around 2 all eigenmodes are stable (see figure 2 in comparison with figure 1). This shows that, within the proposed methodology, the range of control gain $\gamma \sim 2$,

say ($1.5 \leqslant \gamma \leqslant 2.5$), indeed provides the most effective feedback stabilization of the base flow for a very wide range of swirl ratios above ω_1. Present computations show flow stabilization up to 50 % above the critical swirl and indicate that this stabilization can be further increased to much higher swirl ratios.

The analysis of the shape of eigenmodes of the least stable modes sheds light on the special properties and the stabilization mechanism of the feedback control method as control gain γ varies (see figures 4 and 5). It is found that the dispersion of perturbations dominates the flow stabilization when either γ is greater but close to 1 and when $\gamma \gg 1$. On the other hand, when $\gamma = 2$ or around it, flow stabilization is dominated by the feedback control command and therefore is the most effective. We also demonstrate through numerical computations the robustness of the proposed control law to stabilize the solid-body rotation flow in response to both initial waves and continuous inlet flow perturbations and eliminate the vortex breakdown process (see figure 6–9).

Although the control theory in this paper is established largely based on analysis of the solid-body rotation flow, the present results together with Rusak *et al.* (2012) results apply through rescaling to the feedback stabilization of a general swirling flow (with any core size) in a finite-length long pipe with the swirl level close to ω_1. The feedback control is able to overcome the production of the perturbation's energy from both the boundaries and the bulk. Specifically, the result of the potentially best gain $\gamma = 2$ applies for the control of all vortices and is independent of core size (see Xu 2012). Moreover, the analysis of the control of the solid-body rotation flow in a finite-length pipe (that is not necessarily long) using the full linear control problem is representative of the control of vortices with medium to large size cores (where core radius is greater than 50 % of the pipe radius; see Rusak *et al.* 2012). These vortices share a similar linear evolution stage of perturbations as that in the solid-body rotation flow with small production of perturbation's kinetic energy in the domain. Therefore, the present control methodology can stabilize these flows as long as linear dynamics applies. For swirling flow in a short pipe ($L < 3$) with narrow vortex core size, the radial and axial perturbations are more closely coupled and a more complicated energy production mechanism is involved. The proposed control method may have to be modified to regain an effective control for such cases.

Appendix A

We prove the basic energy identities (4.4) and (4.5) for the long-wave (long-pipe) linear control problem.

THEOREM A. *For the control problem (4.1),*

(A.1) when either $c_1 = 1$ *and* $c_2 = 0$ *or* $c_1 = 0$ *and* $c_2 = 1$, *the following energy identity holds,*

$$2\Omega_B \frac{\mathrm{d}}{\mathrm{d}t^*}\tilde{E}(t^*) = -\frac{1}{2}(A_{XX}(1,t^*))^2 - 2\kappa_\omega (A_X(1,t^*))^2 + 2\kappa_\omega (A_X(0,t^*))^2 + A_X(0,t^*)u(t^*); \tag{A 1}$$

(A.2) when $c_1 > 0$, $c_2 > 0$ *and* $c_1 + c_2 = 1$, *the extended energy identity holds,*

$$2\Omega_B \frac{\mathrm{d}}{\mathrm{d}t^*}\hat{E}(t^*) = -\frac{1}{2}(A_{XX}(1,t^*))^2 - 2\kappa_\omega (A_X(1,t^*))^2 + 2\kappa_\omega (A_X(0,t^*))^2 + A_X(0,t^*)u(t^*). \tag{A 2}$$

Proof. We multiply (4.1) by A_{XX} and integrate the result over the interval $0 \leqslant X \leqslant 1$. The left-hand side of the resulting identity becomes

$$\int_0^1 A_{XX}A_{t^*}\,\mathrm{d}X = [A_X A_{t^*}]_{X=0}^{X=1} - \int_0^1 A_X A_{Xt^*}\,\mathrm{d}X. \tag{A 3}$$

For the case where either $c_1 = 1$ and $c_2 = 0$ or $c_1 = 0$ and $c_2 = 1$, and using (4.2), we find

$$\int_0^1 A_{XX}A_{t^*}\,\mathrm{d}X = -\int_0^1 A_X A_{Xt^*}\,\mathrm{d}X = -\frac{1}{2}\int_0^1 [(A_X)^2]_{t^*}\,\mathrm{d}X = -\frac{\mathrm{d}\tilde{E}}{\mathrm{d}t^*}. \tag{A 4}$$

For the case where $c_1 > 0$, $c_2 > 0$, $c_1 + c_2 = 1$, we obtain

$$\int_0^1 A_{XX}A_{t^*}\,\mathrm{d}X = A_X(1,t^*)A_{t^*}(1,t^*) - \int_0^1 A_X A_{Xt^*}\,\mathrm{d}X. \tag{A 5}$$

Note that in this case the boundary term does not vanish at the outlet $X = 1$. However, using the outlet boundary condition in (4.1), we find that

$$A_X(1,t^*)A_{t^*}(1,t^*) = -\frac{c_1}{c_2}A_X(1,t^*)A_{Xt^*}(1,t^*). \tag{A 6}$$

Using (4.3), we find

$$\int_0^1 A_{XX}A_{t^*}\,\mathrm{d}X = -\frac{c_1}{c_2}A_X(1,t^*)A_{Xt^*}(1,t^*) - \int_0^1 A_X A_{Xt^*}\,\mathrm{d}X = -\frac{\mathrm{d}\hat{E}}{\mathrm{d}t^*}. \tag{A 7}$$

The right-hand side of the resulting identities contain the following terms

$$\int_0^1 A_{XX}A_{XXX}\,\mathrm{d}X = \frac{1}{2}[(A_{XX})^2]_{X=0}^{X=1} = \frac{1}{2}(A_{XX}(1,t^*))^2, \tag{A 8}$$

$$\int_0^1 A_{XX}A_X\,\mathrm{d}X = \frac{1}{2}[(A_X)^2]_{X=0}^{X=1}\,\mathrm{d}X = \frac{1}{2}(A_X(1,t^*))^2 - \frac{1}{2}(A_X(0,t^*))^2, \tag{A 9}$$

and

$$\int_0^1 A_{XX}c(X)u(t^*)\,\mathrm{d}X = u(t^*)A_X(X,t^*)c(X)|_{X=0}^{X=1} - \int_0^1 A_X c'(X)u(t^*)\,\mathrm{d}X. \tag{A 10}$$

With putting these terms together we obtain

$$\begin{aligned} 2\Omega_B\frac{\mathrm{d}\tilde{E}}{\mathrm{d}t^*} = &-\frac{1}{2}(A_{XX}(1,t^*))^2 - 2\kappa_\omega(A_X(1,t^*))^2 + 2\kappa_\omega(A_X(0,t^*))^2 \\ &- u(t^*)A_X(X,t^*)c(X)|_{X=0}^{X=1} + \int_0^1 A_X c'(X)u(t^*)\,\mathrm{d}X, \end{aligned} \tag{A 11}$$

for the case where $c_1 = 1$ and $c_2 = 0$ or $c_1 = 0$ and $c_2 = 1$; and

$$\begin{aligned} 2\Omega_B\frac{\mathrm{d}\hat{E}}{\mathrm{d}t^*} = &-\frac{1}{2}(A_{XX}(1,t^*))^2 - 2\kappa_\omega(A_X(1,t^*))^2 + 2\kappa_\omega(A_X(0,t^*))^2 \\ &-u(t^*)A_X(X,t^*)c(X)|_{X=0}^{X=1} + \int_0^1 A_X c'(X)u(t^*)\,\mathrm{d}X. \end{aligned} \tag{A 12}$$

for the case where $c_1 > 0$, $c_2 > 0$ and $c_1 + c_2 = 1$.

Inserting $c(X) = 1 - c_2 X$ into (A 11) and (A 12) and noting that $c_1 + c_2 = 1$ and $c_1 A_X(1, t^*) + c_2 A(1, t^*) = 0$, one obtains the formulas (4.4) and (4.5).

Appendix B

THEOREM B. *For the eigenvalue problem (4.28), the eigenfunction $\tilde{\mathscr{A}}$ and eigenvalues σ^* obey the following relationship (4.29):*

$$\frac{1}{2}\tilde{\mathscr{A}}_{XX}^2(1) + \frac{1}{2}(\gamma - 1)\frac{\Omega - \Omega_B}{\epsilon_1}\tilde{\mathscr{A}}_X^2(0) + \frac{1}{2}\epsilon_1^2\sigma^{*2}\tilde{\mathscr{A}}_X^2(0) + \frac{1}{2}\epsilon_1\Omega_B\sigma^{*2}\tilde{\mathscr{A}}^2(1)$$
$$= -\sigma^* \int_0^1 (2\Omega_B\tilde{\mathscr{A}}_X^2 + 2\epsilon_1\tilde{\mathscr{A}}_{XX}^2)\,\mathrm{d}X. \tag{B 1}$$

Proof. Integrating (4.28) with respect to X over the interval $(0, X)$ and using the boundary conditions leads to

$$\tilde{\mathscr{A}}_{XXX} + \frac{\Omega - \Omega_B}{\epsilon_1}\tilde{\mathscr{A}}_X - \frac{\gamma}{2}\frac{\Omega - \Omega_B}{\epsilon_1}\tilde{\mathscr{A}}_X(0) - 2\Omega_B\sigma^*\tilde{\mathscr{A}} + 2\epsilon_1\sigma^*\tilde{\mathscr{A}}_{XX}$$
$$+ \epsilon_1^2\sigma^{*2}(\tilde{\mathscr{A}}_X - \tilde{\mathscr{A}}_X(0)) - \epsilon_1\Omega_B\sigma^{*2}\int_0^X \tilde{\mathscr{A}}(s)\,\mathrm{d}s = 0. \tag{B 2}$$

$$\tilde{\mathscr{A}}(0) = 0, \quad \tilde{\mathscr{A}}_{XX}(0) = 0 \quad \text{and} \quad \tilde{\mathscr{A}}_X(1) = 0. \tag{B 3}$$

We multiply (B 2) by $\tilde{\mathscr{A}}_{XX}$ and integrate the result over the interval $(0, 1)$. By direct integration and application of the boundary conditions, one finds

$$\int_0^1 \tilde{\mathscr{A}}_{XXX}\tilde{\mathscr{A}}_{XX}\,\mathrm{d}X = \frac{1}{2}\tilde{\mathscr{A}}_{XX}^2(1), \tag{B 4}$$

$$\int_0^1 \tilde{\mathscr{A}}_X\tilde{\mathscr{A}}_{XX}\,\mathrm{d}X = -\frac{1}{2}\tilde{\mathscr{A}}_X^2(0), \tag{B 5}$$

$$\int_0^1 \tilde{\mathscr{A}}_{XX}\,\mathrm{d}X = -\tilde{\mathscr{A}}_X(0), \tag{B 6}$$

$$\int_0^1 \tilde{\mathscr{A}}\tilde{\mathscr{A}}_{XX}\,\mathrm{d}X = [\tilde{\mathscr{A}}\tilde{\mathscr{A}}_X]_0^1 - \int_0^1 \tilde{\mathscr{A}}_X^2\,\mathrm{d}X = -\int_0^1 \tilde{\mathscr{A}}_X^2\,\mathrm{d}X, \tag{B 7}$$

$$\int_0^1 (\tilde{\mathscr{A}}_X - \tilde{\mathscr{A}}_X(0))\tilde{\mathscr{A}}_{XX}\,\mathrm{d}X = \int_0^1 \tilde{\mathscr{A}}_X\tilde{\mathscr{A}}_{XX}\,\mathrm{d}X - \int_0^1 \tilde{\mathscr{A}}_X(0)\tilde{\mathscr{A}}_{XX}\,\mathrm{d}X$$
$$= -\frac{1}{2}\tilde{\mathscr{A}}_X^2(0) - \tilde{\mathscr{A}}_X(0)[\tilde{\mathscr{A}}_X(1) - \tilde{\mathscr{A}}_X(0)] = \frac{1}{2}\tilde{\mathscr{A}}_X^2(0). \tag{B 8}$$

Also integrating in parts shows that

$$\int_0^1 \tilde{\mathscr{A}}_{XX}\left(\int_0^X \tilde{\mathscr{A}}(s)\mathrm{d}s\right)\mathrm{d}X = \left[\tilde{\mathscr{A}}_X\int_0^X \tilde{\mathscr{A}}(s)\,\mathrm{d}s\right]_0^1 - \int_0^1 \tilde{\mathscr{A}}(X)\tilde{\mathscr{A}}_X\,\mathrm{d}X = -\frac{1}{2}\tilde{\mathscr{A}}^2(1). \tag{B 9}$$

Combining (B 4)–(B 9), one obtains (4.29).

REFERENCES

BENJAMIN, T. B. 1962 Theory of the vortex breakdown phenomenon. *J. Fluid Mech.* **14**, 593–629.

BERAN, P. S. 1994 The time-asymptotic behaviour of vortex breakdown in tubes. *Comput. Fluids* **23**, 913–937.

BERAN, P. S. & CULICK, F. E. C. 1992 The role of non-uniqueness in the development of vortex breakdown in tubes. *J. Fluid Mech.* **242**, 491–527.

BRÜCKER, CH. & ALTHAUS, W. 1995 Study of vortex breakdown by particle tracking velocimetry (PTV), Part 3: time-dependent structure and development of breakdown modes. *Exp. Fluids* **18**, 174–186.

DELERY, J. M. 1994 Aspects of vortex breakdown. *Prog. Aerosp.* **30** (1), 1–59.

FALER, J. H. & LEIBOVICH, S. 1977 Disrupted states of vortex flow and vortex breakdown. *J. Phys. Fluids* **20**, 1385–1400.

GALLAIRE, F., CHOMAZ, J.-M. & HUERRE, P. 2004 Closed-loop control of vortex breakdown: a model study. *J. Fluid Mech.* **511**, 67–93.

GARG, A. K. & LEIBOVICH, S. 1979 Spectral characteristics of vortex breakdown flow fields. *Phys. Fluids* **22**, 2053.

HALL, M. G. 1972 Vortex breakdown. *Annu. Rev. Fluid Mech.* **4**, 195–217.

KELVIN, LORD 1880 Vibrations of a columnar vortex. *Phil. Mag.* **10**, 155–168.

KNOLE, M. & SATTELMAYER, T. 2009 Interaction of heat release and vortex breakdown during flame flashback driven by combustion induced vortex breakdown. *Exp. Fluids* **47** (45), 627–635.

LEIBOVICH, S. 1978 The structure of vortex breakdown. *Annu. Rev. Fluid Mech.* **10**, 221–246.

LEIBOVICH, S. 1984 Vortex stability and breakdown: survey and extension. *AIAA J.* **22**, 1192–1206.

LEIBOVICH, S. & RANDALL, J. D. 1972 Solitary waves in concentrated vortices. *J. Fluid Mech.* **52**, 625–635.

LONG, R. R. 1953 Steady motion around a symmetrical obstacle moving along the axis of a rotating liquid. *J. Met.* **10**, 197–203.

LOPEZ, J. M. 1994 On the bifurcation structure of axisymmetric vortex breakdown in a constricted pipe. *Phys. Fluids* **6**, 3683–3693.

MATTNER, T. W., JOUBERT, P. N. & CHONG, M. S. 2002 Vortical flow. Part 1. Flow through a constant diameter pipe. *J. Fluid Mech.* **463**, 259–291.

MELIGA, P. & GALLAIRE, F. 2011 Control of axisymmetric vortex breakdown in a constricted pipe: nonlinear steady states and weakly nonlinear asymptotic expansions. *Phys. Fluids* **23**, 084102.

MITCHELL, A. M. & DELERY, J. 2001 Research into vortex breakdown control. *Prog. Aerosp. Sci.* **37** (4), 385–418.

MURUGANANDAM, T. M., NAIR, S, SCARBOROUGH, D., NEUMEIER, Y, JAGODA, J., LIEUWEN, T., SEITZMAN, J. & ZINN, B. 2005 Active control of lean blowout for turbine engine combustors. *J. Propul. Power* **21** (5), 807–814.

O'NEIL, P. J., ROOS, F. W., BARNETT, R. M. & HAWK, J. D. 1989, Investigation of flow characteristics of developed vortex, McDonnell Aircraft Company, *Report* NADC-89114-60, St Louis, MO.

PASCHEREIT, C. O. & GUTMARK, E. 2002 Proportional control of combustion instabilities in a simulated gas-turbine combustor. *J. Propul. Power* **18** (6), 1298–1304.

PECKHAM, D. H. & ATKINSON, S. A. 1957, Preliminary results of low speed wind tunnel tests on a gothic wing of aspect ratio 1.0, *Technical Report* CP508, Aeronautical Research Council London.

RAYLEIGH, LORD 1916 On the dynamics of revolving fluids. *Proc. R. Soc. Lond. Ser.* A **93**, 148–154.

RUSAK, Z. & LAMB, D. 1999 Prediction of vortex breakdown in leading-edge vortices above slender delta wings. *J. Aircraft* **36** (4), 659–667.

RUSAK, Z., WANG, S. & WHITING, C. H. 1998 The evolution of a perturbed vortex in a pipe to axisymmetric vortex breakdown. *J. Fluid Mech.* **366**, 211–237.

RUSAK, Z., WANG, S., XU, L. & TAYLOR, S. 2012 On the global nonlinear stability of near-critical swirling flow in a long finite-length pipe and the path to vortex breakdown. *J. Fluid Mech.* **712**, 295–326.

RUSAK, Z., WHITING, C. H. & WANG, S. 1998 Axisymmetric breakdown of a Q-vortex in a pipe. *AIAA J.* **36** (10), 1848–1853.

SARPKAYA, T. 1971 On stationary and travelling vortex breakdowns. *J. Fluid Mech.* **45**, 545–559.

SARPKAYA, T. 1995 Turbulent vortex breakdown. *Phys. Fluids* **7** (10), 2301–2303.

SNYDER, D. & SPALL, R. 2000 Numerical simulation of bubble-type vortex breakdown within a tube-and-vane apparatus. *Phys. Fluids* **12** (3), 603–608.

SQUIRE, H. B. 1960 Analysis of the vortex breakdown phenomenon. In *Miszallaneen der Angewandten Mechanik*, pp. 306–312. Akademie.

WANG, S. 2008 A novel method for analysing the global stability of inviscid columnar swirling flow in a finite pipe. *Phys. Fluids* **20**, 074101.

WANG, S. 2009 On the nonlinear stability of inviscid axisymmetric swirling flows in a pipe of finite length. *Phys. Fluids* **21**, 084104.

WANG, S. & RUSAK, Z. 1996 On the stability of an axisymmetric rotating flow in a pipe. *Phys. Fluids* **8** (4), 1007–1016.

WANG, S. & RUSAK, Z. 1997 The dynamics of a swirling flow in a pipe and transition to axisymmetric vortex breakdown. *J. Fluid Mech.* **340**, 177–223.

WANG, S. & RUSAK, Z. 2011 Energy transfer mechanism of the instability of an axisymmetric swirling flow in a finite-length pipe. *J. Fluid Mech.* **679**, 505–543.

XU, L. 2012, Vortex flow stability, dynamics and feedback stabilization. Ph.D. dissertation, Rensselaer Polytechnic Institute.